PTEP

Prog. Theor. Exp. Phys. **2022** 053G01(44 pages)
DOI: 10.1093/ptep/ptac053

Two-dimensional resistive-wall impedance with finite thickness: Its mathematical structures and their physical meanings

Yoshihiro Shobuda

J-PARC Center, JAEA&KEK, 2-4 Shirakata, Tokaimura, Nakagun, Ibaraki 319-1195, Japan
*E-mail: yoshihiro.shobuda@j-parc.jp

Received September 6, 2021; Revised March 7, 2022; Accepted March 17, 2022; Published March 22, 2022

When the skin depth is greater than the chamber thickness for relativistic beams, the two-dimensional longitudinal resistive-wall impedance of a cylindrical chamber with a finite thickness decreases proportionally to the frequency. The phenomenon is commonly interpreted as electromagnetic fields leaking out of the chamber over a frequency range. However, the relationship between the wall current on the chamber and the leakage fields from the chamber is unclear because the naive resistive-wall impedance formula does not dynamically express how the wall current converts to the leakage fields when the skin depth exceeds the chamber thickness. A prestigious textbook [1] re-expressed the resistive-wall impedance via a parallel circuit model with the resistive-wall and inductive terms to provide a dynamic picture of the phenomenon. However, there are some flaws in the formula. This study highlights them from a fundamental standpoint, and provides a more appropriate and rigorous picture of the longitudinal resistive-wall impedance with finite thickness. To demonstrate their physical meaning, we re-express the longitudinal impedance for non-relativistic beams, as well as the transverse resistive-wall impedance including space charge impedance based on a parallel circuit model.

Subject Index G13, G15

1. Introduction

Resistive-wall impedances can be a significant source of beam instabilities [1,2]. As a result, many researchers [3–21] have extensively studied the longitudinal and transverse resistive-wall impedances of an infinitely long multi-layered chamber. It is fundamentally a two-dimensional problem that can be solved using field-matching techniques [1, Chap. 9].

The longitudinal impedance [2] for a "2-dimensional" cylindrical resistive chamber with a very thin wall at low frequencies is expressed by the equivalent circuit consisting of the parallel circuit of the "DC" constant resistance and the inductance caused by the displacement current flowing outside the wall proper for relativistic beams, according to a prestigious textbook [1, Appendix 6.A] on beam coupling impedances in accelerator physics. However, the applicability conditions of this formula are not so clear, because the well-known conventional resistive-wall impedance for the finite-thickness chamber monotonically approaches zero toward the frequency origin [2], and there is no frequency region in which the direct current (DC) constant resistance plays a significant role, even when the skin depth is greater than the chamber thickness.

The beam impedance of the authors' "2.5-dimensional" short ceramic break with titanium nitride coating sandwiched between perfectly conductive chambers, on the other hand, successfully describes the impedance in terms of the electric circuit model consisting of three electric components in parallel: the resistive-wall term, the displacement current term in the ceramic, and the radiation term [22]. When the skin depth is greater than the thickness of the titanium nitride, the real part of the impedance reproduces the DC resistance in the formula, except in an extremely thin case (typically less than a nanometre) where the radiation effects become dominant over the wall-current effects. The expression of the impedance from the perspective of the parallel electric circuit model is certainly intuitive because we can naturally understand that the impedance of the ceramic break is determined to minimize the energy loss of the beam, which is smaller when the wall current runs on the thin titanium nitride with high resistance than when it converts to radiation out to free space (gap impedance [23]), when the beam passes through the ceramic break except for the extremely thin titanium-nitride-coated case.

We re-investigate in this report how the longitudinal resistive-wall impedance of a two-dimensional cylindrical chamber for relativistic beams is described in the prestigious textbook [1, Appendix 6.A] by the equivalent circuit consisting of the parallel circuit of the DC constant resistance and the inductance caused by the displacement current flowing outside the wall proper. Starting with the rigorous formula, we survey the mathematical structure of the two-dimensional resistive-wall impedance including non-relativistic space charge effects. As a result, we point out some shortcomings of the previous formula and present a more appropriate physical representation of the resistive-wall impedance with finite thickness in terms of the electric circuit model.

Similarly, we revisit the longitudinal impedance, even for non-relativistic beams, as well as the transverse resistive-wall impedance, including space charge impedance, beginning with the rigorous formula, to comprehend their physical meaning. Finally, it is obvious that the longitudinal and transverse resistive-wall impedances are chosen to minimize the energy loss of the beam, regardless of whether the beam is relativistic or not, as in the case of a 2.5-dimensional short ceramic break with titanium nitride coating. In contrast to the longitudinal impedance for relativistic beams, the DC constant resistance appears in the impedances for non-relativistic beams to minimize the beam's energy loss.

In Sect. 2, to properly distinguish between the 2.5-dimensional of the short ceramic break and the 2-dimensional resistive chamber, we compare the characteristics of the ceramic break's impedance with those of the conventional resistive-wall impedance, and observe some unclear features about the chamber thickness dependence on the resistive-wall impedance. In Sect. 3 we present the rigorous formula for the longitudinal resistive-wall impedance for a finite-thickness chamber with an outer surface covered by a vacuum layer that is further enclosed by an infinitely thick perfectly conductive chamber. Based on the rigorous formula, we modify some of the shortcomings of the previous picture of the resistive-wall impedance for relativistic beams. We generalize the scheme to the longitudinal impedance of non-relativistic beams at the end of this section. In Sect. 4, we present the rigorous formula for transverse resistive-wall impedance and examine the characteristic in the same way. Section 5 summarizes the research.

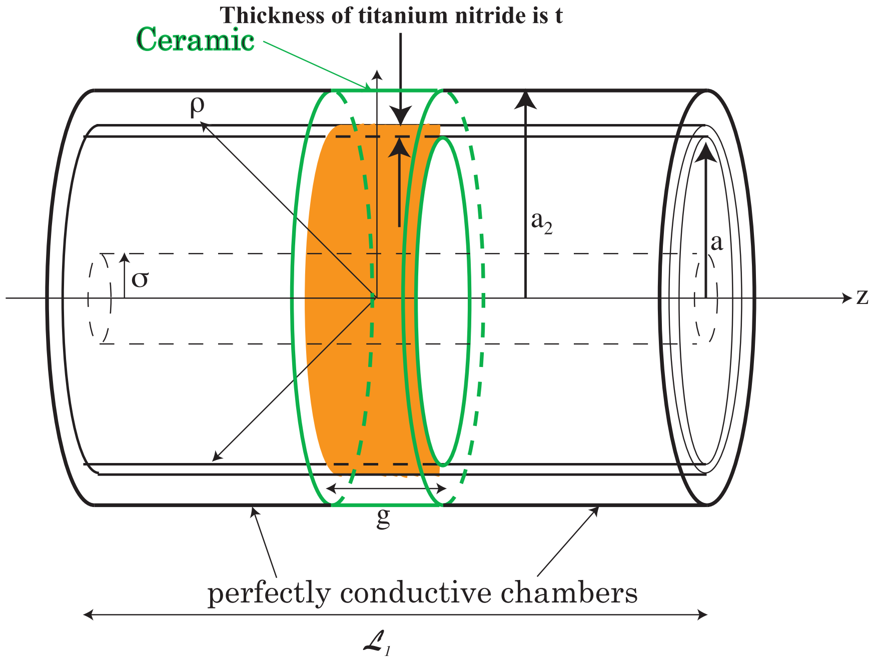

Fig. 1. Schematic of a short ceramic break with a titanium nitride coating sandwiched between two perfectly conductive chambers.

2. Longitudinal impedance of a titanium-nitride-coated short ceramic break and the conventional formula for a resistive cylindrical chamber

Consider the situation depicted in Fig. 1, in which a cylindrical beam with radius σ passes through a titanium-nitride-coated short ceramic break of length g (typically $\sim$10 mm) sandwiched by two perfectly conductive chambers of length $(\mathcal{L}_1 - g)/2$. In this case, the longitudinal impedance of the ceramic break at low frequencies is approximated by adding in parallel the impedances of the resistive wall caused by the titanium nitride coating, the radiation, and the ceramic capacitor [22].

In particular, when the ceramic break's longitudinal impedance $Z_{\mathrm{L}}^{(c)}$ is defined as the average of the longitudinal electric field (normalized by the beam current) over the beam's cross-section, including the "non-relativistic" space charge impedance $Z_{\mathrm{non,\,sp}}(a)$ for the perfectly conductive chamber of radius a and length $\mathcal{L}_1$ [21],

$$Z_{\mathrm{non,sp}}(a) = -\mathcal{L}_1 \frac{j2Z_0\left[\frac{1}{2} - I_1(\bar{k}\sigma)K_1(\bar{k}\sigma) - \frac{K_0(\bar{k}a)I_1^2(\bar{k}\sigma)}{I_0(\bar{k}a)}\right]}{\bar{k}\beta\gamma\pi\sigma^2}, \tag{1}$$

the total longitudinal impedance at low frequencies ($f \ll c/\pi g$) is expressed as

$$Z_{\mathrm{L}}^{(c)} = Z_{\mathrm{non,sp}}(a) + Z_{\mathrm{cerTiN,L}}^{(\sigma)}, \tag{2}$$

where

$$Z_{\mathrm{cerTiN,L}}^{(\sigma)} \simeq \mathcal{F}^{(\sigma)} \frac{a_2}{aI_0^2(\bar{k}a)} \frac{\sin^2\left(\frac{kg}{2}\right)}{\left(\frac{kg}{2}\right)^2} \left[\frac{jk\beta a_2(\langle J(z)\rangle + \langle Y(z)\rangle)}{Z_0} - \frac{j2\pi a_2 \kappa_{\mathrm{TiN}} \tanh \kappa_{\mathrm{TiN}} t}{gk\beta Z_0} + \frac{j2\omega\epsilon_1 \pi a_2(a_2 - a)}{cZ_0 g}\right]^{-1}; \tag{3}$$

$$\mathcal{F}^{(\sigma)} = \frac{4I_1^2(\bar{k}\sigma)}{\bar{k}^2\sigma^2}; \tag{4}$$

$$\kappa_{\rm TiN} = \sqrt{jk\beta Z_0\sigma_{2c}}; \tag{5}$$

$$\langle J(z)\rangle = -\sum_{s=1}^{\infty}\frac{4\pi a}{gb_s^2} - \sum_{s=1}^{\infty}\frac{4\pi a^2(e^{-j\frac{b_s}{a}g}-1)}{jg^2b_s^3}; \tag{6}$$

$$\langle Y(z)\rangle = -\int_0^{\infty} d\zeta\, \frac{4}{g\pi a_2\zeta\left(k^2\beta^2+\frac{\zeta}{a_2^2}\right)H_0^{(1)}(e^{j\frac{\pi}{2}}\sqrt{\zeta})H_0^{(2)}(e^{j\frac{\pi}{2}}\sqrt{\zeta})}$$
$$-\int_0^{\infty} d\zeta\, \frac{4(e^{-jg\sqrt{k^2\beta^2+\frac{\zeta}{a_2^2}}}-1)}{jg^2\pi a_2\zeta\left(k^2\beta^2+\frac{\zeta}{a_2^2}\right)^{\frac{3}{2}}H_0^{(1)}(e^{j\frac{\pi}{2}}\sqrt{\zeta})H_0^{(2)}(e^{j\frac{\pi}{2}}\sqrt{\zeta})}; \tag{7}$$

$b_s^2 = k^2\beta^2a^2 - j_{0,s}^2 = -\beta_s^2$, and b_s approaches $-j\beta_s$ for $j_{0,\,s} > k\beta a$; j_{s0} are the sth zeros of $J_0(z)$; $J_0(z)$ is the Bessel function; $H_m^{(1)}$ and $H_m^{(2)}$ are the Hankel functions of the first and second kinds [24]; $Z_0 = 120\pi$ [Ω] is the free space impedance; j is the imaginary unit; a and a_2 are the inner and the outer radii of the chamber; t is the thickness of the titanium nitride; ϵ_1 is the relative dielectric constant of the ceramic; μ_1 is the relative permeability of the ceramic, which is assumed to be 1; σ_{2c} is the conductivity of the titanium nitride; c is the velocity of light; ω is the angular frequency; β and γ are the Lorentz β and γ; $k = \omega/c\beta$; and $\bar{k} = k/\gamma$.

Except for the space charge impedance $Z_{\rm non,\,sp}(a)$, the ceramic break impedance is described by Eq. (3) where the effect of the radial size of the beam σ is factorized in $\mathcal{F}^{(\sigma)}$ approaching 1 for infinitesimal σ.

Let us focus on the ceramic break with $a_2 \approx a$. The first term in the denominator of $Z_{\rm cerTiN,L}^{(\sigma)}$ represents the admittance of radiation effects out to free space as well as into the chamber, which is caused by the conversion of a portion of the wall-current as the beam passes through the ceramic break. The second term refers to the titanium nitride's resistive-wall admittance. The ceramic break admittance is the third term in the denominator, because the capacitance $C_{\rm cer}$ caused by the ceramic break is approximated as

$$C_{\rm cer} = \frac{\epsilon_1\pi(a_2+a+t)(a_2-a-t)}{cZ_0g} \simeq \frac{2\epsilon_1\pi a_2(a_2-a)}{cZ_0g}. \tag{8}$$

The description of the impedance is intuitively appealing because we can see that the impedance is determined by minimizing the energy loss of the beam.

To be more specific, for the titanium nitride coating (typically larger than a few tens of nanometres) as

$$t > t_{\rm min} = \left(\frac{4g}{\pi^2Z_0^3\sigma_{2c}^3}\right)^{\frac{1}{4}}, \tag{9}$$

and less than skin depth δ,

$$\delta = \sqrt{\frac{2}{\mu'\mu_0\sigma_{2c}\omega}}, \tag{10}$$

where μ' is the relative permeability of titanium nitride, which is assumed to be 1, the effect of radiation terms such as $<J>$ and $<Y>$ is ignored at low frequencies. That is, the real part of

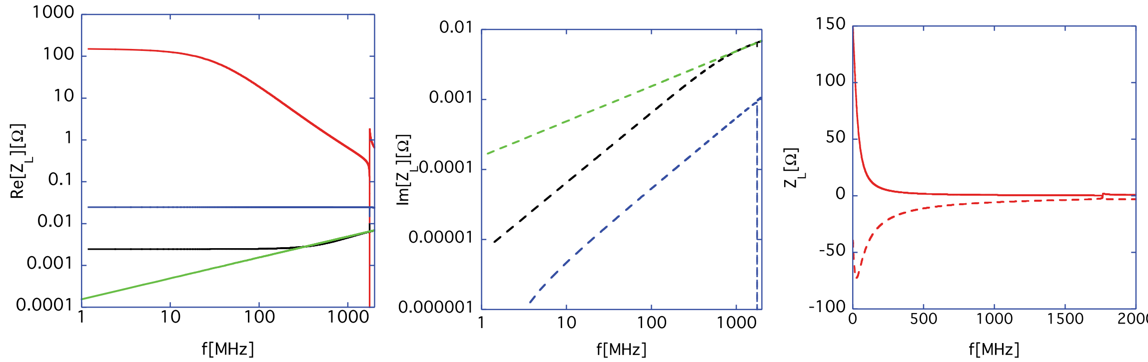

Fig. 2. Longitudinal impedance by Eq. (3) (red, blue, and black) for a relativistic pencil beam ($\sigma = 0\,\mathrm{m}$), and the conventional formula of Eq. (12) (green), where $\gamma = 1000$, $a = 65\,\mathrm{mm}$, $a_2 = 70\,\mathrm{mm}$, $\sigma_{2c} = 10^5\,\mathrm{S\,m^{-1}}$, $g = 10\,\mathrm{mm}$, and $\epsilon_1 = 11$. We symbolically represent Z_{L} on the vertical axis as the longitudinal impedance. The solid and dashed lines show the real and imaginary parts of the impedances, respectively. The red, blue, and black lines show the results with $t = 1\,\mathrm{nm}$, $t = 10\,\mu\mathrm{m}$, and $t = 100\,\mu\mathrm{m}$, respectively.

the impedance approaches the titanium nitride coating's DC resistance,

$$Z^{(\sigma)}_{\mathrm{cerTiN,L}} = \frac{g}{\sigma_{2c} 2\pi a t}, \tag{11}$$

for a relativistic pencil beam, as evidenced by measurements [18]. Meanwhile, $Z^{(\sigma=0)}_{\mathrm{cerTiN,L}}$ for a "thick" titanium nitride coating, where $\delta < t$, reproduces the traditional resistive-wall impedance formula with "infinite" thickness as [2,17]

$$Z^{(\sigma=0)}_{\mathrm{cerTiN,L}} = g Z_0 \frac{(1+j)}{4\pi a}\sqrt{\frac{2\omega}{c Z_0 \sigma_{2c}}}. \tag{12}$$

For an ultrathin titanium nitride coating (typically $\sim$ a nanometre) with

$$t \ll t_{\min}, \tag{13}$$

instead of the resistive-wall part, the radiation terms play an important role in the impedance in most frequency regions, because the energy loss of the beam becomes smaller, thanks to the conversion of wall-current into the radiation fields rather than staying in the ultrathin titanium nitride.

Figure 2 depicts the longitudinal impedance $Z^{(\sigma)}_{\mathrm{cerTiN,L}}$ by Eq. (3) (red, blue, and black) for a relativistic pencil beam ($\sigma = 0\,\mathrm{m}$), as well as the conventional formula of Eq. (12) (green) with infinite thickness, where $\gamma = 1000$, $a = 65\,\mathrm{mm}$, $a_2 = 70\,\mathrm{mm}$, $\sigma_{2c} = 10^5\,\mathrm{S\,m^{-1}}$, $g = 10\,\mathrm{mm}$, and $\epsilon_1 = 11$. The solid and dashed lines show the real and imaginary parts of the impedance, respectively. The red, blue, and black lines represent the results obtained with $t = 1\,\mathrm{nm}$, $t = 10\,\mu\mathrm{m}$, and $t = 100\,\mu\mathrm{m}$, respectively.

Except for the case of extremely thin titanium nitride (red), the real part of the impedance is identical with the DC resistance in the frequency range where the skin depth δ is greater than the thickness of the titanium nitride t, as shown in the left panel. When the skin depth is greater than the thickness of the titanium nitride, the wall-current continues to flow in the titanium nitride. As a result, the middle figure depicts how the imaginary part of the impedance is more suppressed as the titanium nitride becomes thinner as opposed to the conventional impedance (green dashed). In both left and middle panels we can see how the impedance for $t = 100\,\mu\mathrm{m}$ (black) differs from the conventional resistive-wall impedance (green) below $f = 250\,\mathrm{MHz}$ ($\delta > t$).

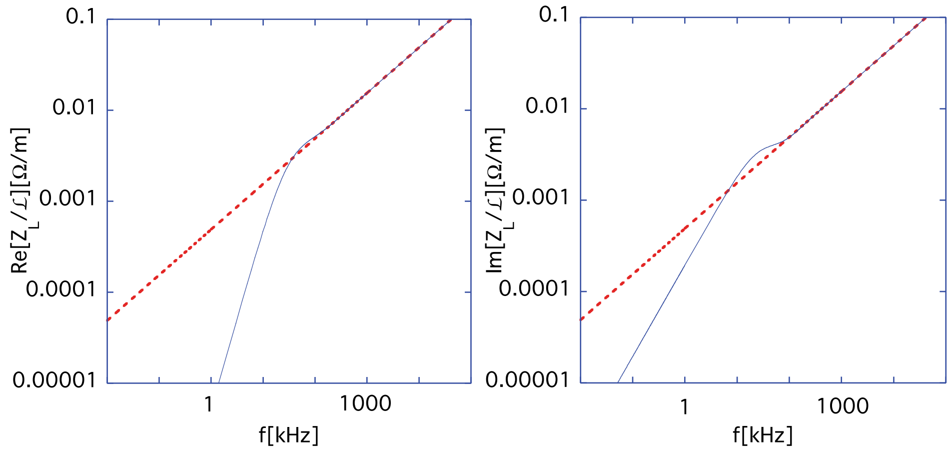

Fig. 3. Comparisons of the longitudinal impedance as calculated by Eq. (12) with g replaced by $\mathcal{L}$ (red dashed), and as calculated by Eq. (15) with $t = 10$ mm (blue solid). We symbolically represent Z_L on the vertical axis as the longitudinal impedance. The parameters for both cases are $a = 65$ mm and $\sigma_{2c} = 10^5\,\mathrm{S\,m^{-1}}$.

The impedance for extremely thin titanium nitride ($t = 1$ nm), in the right panel, is well approximated by a ceramic gap impedance [22], so that the imaginary part of the impedance becomes capacitive and the cut-off frequency (1.76 GHz) is identified (we can identify the cut-off frequency on the blue lines in the left and middle panels, as well). Nature tries to minimize the energy loss of the beam, so the radiation fields play an important role in this case. Indeed, the titanium nitride's DC resistance $g/\sigma_{2c}2\pi at = 245\,\Omega$ is greater than the maximum value of the real part of the impedance, 150 Ω (see the left panel).

The conventional resistive-wall impedance $Z_{\mathrm{res}}^{(\mathrm{con})}$ of a two-dimensional cylindrical chamber with inner radius a, "finite" thickness t, and length $\mathcal{L}$, except for the conventional relativistic space charge impedance,

$$Z_{\mathrm{rel,sp}}^{(\mathrm{con})} = -\frac{j\omega\mathcal{L}Z_0}{4\pi c\beta^2\gamma^2}g_f, \tag{14}$$

is given by [2]

$$Z_{\mathrm{res}}^{(\mathrm{con})} = \mathcal{G}\mathcal{L}Z_0\frac{(1+j)}{4\pi a}\sqrt{\frac{2\omega}{cZ_0\sigma_{2c}}}, \tag{15}$$

where $\mu_0 = Z_0/c$ denotes the vacuum permeability,

$$\mathcal{G} = \tanh\left[(1+j)\sqrt{\frac{\omega\mu_0\sigma_{2c}}{2}}t\right], \tag{16}$$

is the geometric factor, and

$$g_f = 1 + 2\log\left[\frac{a}{\sigma}\right], \tag{17}$$

is the g-factor describing the space charge impedance [2]. Here, it is clear that the factor $\mathcal{G}$ approaches 1 as the thickness t approaches infinity.

Figure 3 shows a comparison of the longitudinal impedance calculated by Eq. (12) with g replaced by $\mathcal{L}$ (red dashed), and Eq. (15) with $t = 10$ mm (blue solid). In both cases, the parameters are $a = 65$ mm and the chamber conductivity $\sigma_{2c} = 10^5\,\mathrm{S\,m^{-1}}$ (corresponding to titanium nitride on the ceramic break).

Due to the geometric factor $\mathcal{G}$, the impedance $Z_{\rm res}^{\rm (con)}$ from Eq. (15) reproduces the conventional resistive-wall impedance formula of Eq. (12) for a thick chamber $\delta < t$, whereas $Z_{\rm res}^{\rm (con)}$ is approximated for thin chambers as

$$Z_{\rm res}^{\rm (con)} = j\omega \frac{Z_0}{c}\frac{1}{2\pi a}\mathcal{L}t. \tag{18}$$

Because it represents the magnetic flux originating from the beam and penetrating the thin wall, Eq. (18) has a very different physical meaning from Eq. (11). Although the conventional formula in Eq. (15) for the resistive-wall impedance approaches zero for infinitesimal t, the mechanism of how the resistive-wall impedance converts to leakage (radiation) fields, as well as how the assumed space charge impedance from Eq. (14) is modified for an extremely thin chamber after being affected by the leakage fields, remains unclear.

This confusion may be clarified by introducing an additional layer outside the resistive chamber, because Ref. [22] demonstrates that the longitudinal impedance of a ceramic break whose inner surface is coated with titanium nitride and "whose outer surface is additionally covered over perfectly conductive wall" approaches the impedance of an infinitely long titanium-nitride-coated ceramic chamber covered by a perfectly conductive wall (refer to Appendix B) [25],

$$Z_{\rm L} = \mathcal{L}Z_0\left[2\pi\beta a\left(Z_0 t\sigma_{2c} - \frac{j\epsilon_1}{(\epsilon_1\beta^2-1)ka\log\frac{a_2}{a}}\right)\right]^{-1}, \tag{19}$$

as the length of the ceramic break ($g = \mathcal{L}$) approaches infinity. It is clear that Eq. (19) returns to zero at zero frequency, regardless of whether t is finite or not, recapturing the characteristic of Eq. (15): conventional resistive-wall impedance.

Let us revisit the longitudinal resistive-wall impedance of a two-dimensional cylindrical chamber in the following section by introducing a perfectly conductive wall outside the resistive chamber.

3. Longitudinal resistive-wall impedance of a two-dimensional cylindrical chamber

3.1 *Overview of the longitudinal resistive-wall impedance*

Let us now concentrate on the resistive-wall impedance of a two-dimensional cylindrical chamber of length $\mathcal{L}$, inner radius a, and thickness t. As shown in Fig. 4, we add an infinitely thick perfectly conductive chamber with inner radius $d\,(>a+t)$ outside the resistive chamber, where the space between the inner wall at $\rho = a + t$ and the outer one at $\rho = d$ in the radial ρ-direction is filled with a vacuum.

To begin, we will go over the rigorous formula for the longitudinal resistive-wall impedance obtained by solving the Maxwell equations (see Appendices A1 and A2). When the longitudinal impedance is defined as the average of the longitudinal electric field (normalized by the beam current) over the beam's cross-section, the total longitudinal impedance $Z_{\rm L}^{R}$, including the non-relativistic space charge impedance $Z_{\rm non,\,sp}(a)$ (compare Eqs. (1) and (21)) is given as

$$\frac{Z_{\rm L}^{R}}{\mathcal{L}} = \frac{Z_{\rm non,sp}(a)}{\mathcal{L}} + \frac{Z_{\rm RW,rig}}{\mathcal{L}}, \tag{20}$$

where

$$\frac{Z_{\rm non,sp}(a)}{\mathcal{L}} = -\frac{j2Z_0\left[\frac{1}{2} - I_1(\bar{k}\sigma)K_1(\bar{k}\sigma) - \frac{K_0(\bar{k}a)I_1^2(\bar{k}\sigma)}{I_0(\bar{k}a)}\right]}{\bar{k}\beta\gamma\pi\sigma^2}; \tag{21}$$

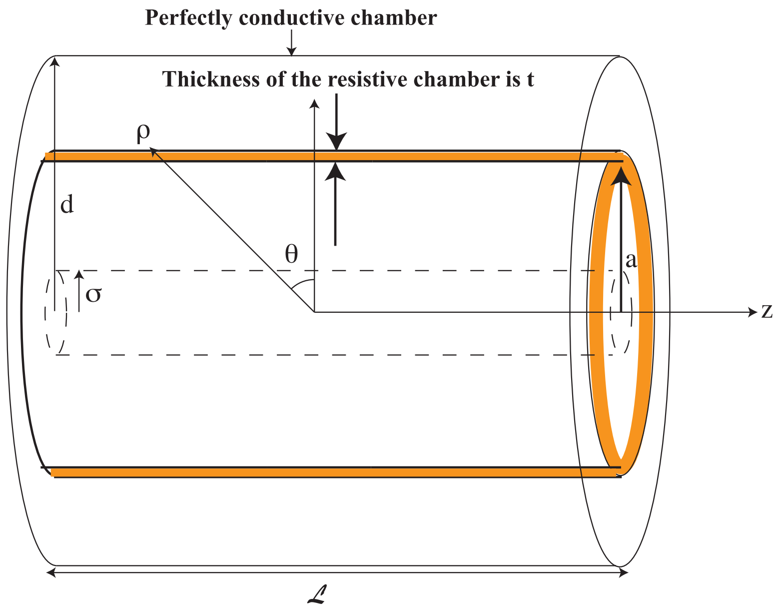

Fig. 4. Schematic picture of a resistive chamber covered by a perfectly conductive chamber through a vacuum layer with a thickness of $d - a - t$.

$$\frac{Z_{\mathrm{RW,rig}}}{\mathcal{L}} = -\frac{j2Z_0K_0(\bar{k}a)I_1^2(\bar{k}\sigma)}{\bar{k}\pi\beta\gamma\sigma^2 I_0(\bar{k}a)} - \frac{2I_1^2\left(\bar{k}\sigma\right)jZ_0\mathcal{N}(k)}{\bar{k}\sigma^2\beta\pi\gamma\mathcal{D}(k)}; \tag{22}$$

$$\begin{aligned}\mathcal{N}(k) = \alpha^{(1)}&\left[Z_0(\sigma_{2c} + j\omega\epsilon'\epsilon_0)K_0(\bar{k}a)I_1(\nu_2 a) + j\beta\gamma\nu_2K_1(\bar{k}a)I_0(\nu_2 a)\right]\\
&- Z_0(\sigma_{2c} + j\omega\epsilon'\epsilon_0)K_0(\bar{k}a)K_1(\nu_2 a) + j\nu_2\beta\gamma K_1(\bar{k}a)K_0(\nu_2 a)\\
&+ \frac{K_0\left(\bar{k}d\right)}{I_0\left(\bar{k}d\right)}\left[\alpha^{(2)}\left(-Z_0(\sigma_{2c} + j\omega\epsilon'\epsilon_0)K_0(\bar{k}a)I_1(\nu_2 a) - j\beta\gamma\nu_2K_1(\bar{k}a)I_0(\nu_2 a)\right)\right.\\
&\left.+ \alpha^{(3)}\left(Z_0(\sigma_{2c} + j\omega\epsilon'\epsilon_0)K_0(\bar{k}a)K_1(\nu_2 a) - j\nu_2\beta\gamma K_1(\bar{k}a)K_0(\nu_2 a)\right)\right];\end{aligned} \tag{23}$$

$$\begin{aligned}\mathcal{D}(k) = \alpha^{(1)}&\left[-(\sigma_{2c} + j\omega\epsilon'\epsilon_0)Z_0I_0\left(\bar{k}a\right)I_1(\nu_2 a) + j\beta\gamma\nu_2I_1\left(\bar{k}a\right)I_0(\nu_2 a)\right]\\
&+ (\sigma_{2c} + j\omega\epsilon'\epsilon_0)Z_0I_0\left(\bar{k}a\right)K_1(\nu_2 a) + j\beta\gamma\nu_2I_1\left(\bar{k}a\right)K_0(\nu_2 a)\\
&+ \frac{K_0\left(\bar{k}d\right)}{I_0\left(\bar{k}d\right)}\left[\alpha^{(2)}\left(Z_0(\sigma_{2c} + j\omega\epsilon'\epsilon_0)I_0\left(\bar{k}a\right)I_1(\nu_2 a) - j\beta\gamma\nu_2I_1\left(\bar{k}a\right)I_0(\nu_2 a)\right)\right.\\
&\left.- \alpha^{(3)}\left(Z_0(\sigma_{2c} + j\omega\epsilon'\epsilon_0)I_0\left(\bar{k}a\right)K_1(\nu_2 a) + j\beta\gamma\nu_2I_1\left(\bar{k}a\right)K_0(\nu_2 a)\right)\right];\end{aligned} \tag{24}$$

$$\alpha^{(1)} = \frac{\left[K_1(\nu_2(a+t)) - \frac{j\beta\gamma\nu_2K_0(\nu_2(a+t))K_1\left(\bar{k}(a+t)\right)}{Z_0(\sigma_{2c}+j\omega\epsilon'\epsilon_0)K_0\left(\bar{k}(a+t)\right)}\right]}{\left[I_1(\nu_2(a+t)) + \frac{j\beta\gamma\nu_2I_0(\nu_2(a+t))K_1\left(\bar{k}(a+t)\right)}{Z_0(\sigma_{2c}+j\omega\epsilon'\epsilon_0)K_0\left(\bar{k}(a+t)\right)}\right]}; \tag{25}$$

$$\alpha^{(2)} = \frac{K_1\left(\nu_2(a+t)\right) I_0\left(\bar{k}(a+t)\right)\left[1+\frac{j\beta\gamma\nu_2 K_0(\nu_2(a+t)) I_1\left(\bar{k}(a+t)\right)}{Z_0(\sigma_{2c}+j\omega\epsilon'\epsilon_0)K_1(\nu_2(a+t))I_0\left(\bar{k}(a+t)\right)}\right]}{I_1\left(\nu_2(a+t)\right) K_0\left(\bar{k}(a+t)\right)\left[1+\frac{j\beta\gamma\nu_2 I_0(\nu_2(a+t)) K_1\left(\bar{k}(a+t)\right)}{Z_0(\sigma_{2c}+j\omega\epsilon'\epsilon_0)I_1(\nu_2(a+t))K_0\left(\bar{k}(a+t)\right)}\right]}; \tag{26}$$

$$\alpha^{(3)} = \frac{\left[I_0\left(\bar{k}(a+t)\right) - \frac{j\beta\gamma\nu_2 I_0(\nu_2(a+t)) I_1\left(\bar{k}(a+t)\right)}{Z_0(\sigma_{2c}+j\omega\epsilon'\epsilon_0)I_1(\nu_2(a+t))}\right]}{\left[K_0\left(\bar{k}(a+t)\right) + \frac{j\beta\gamma\nu_2 I_0(\nu_2(a+t)) K_1\left(\bar{k}(a+t)\right)}{Z_0(\sigma_{2c}+j\omega\epsilon'\epsilon_0)I_1(\nu_2(a+t))}\right]}; \tag{27}$$

$$\nu_2 = \sqrt{k^2(1-\beta^2\epsilon'\mu') + jk\beta\mu' Z_0\sigma_{2c}}; \tag{28}$$

$Z_{\mathrm{RW,\,rig}}$ is the resistive-wall impedance except for space charge effects; $\epsilon_0 = 1/cZ_0$ is the dielectric constant of vacuum; σ_{2c} is the conductivity of the chamber; $\epsilon^{'}$ is the relative dielectric constant of the chamber; $\mu^{'}$ is the relative permeability of the chamber; and $I_n(z)$ and $K_n(z)$ are the modified Bessel functions [24].

We can reproduce the previous expression for the impedance Z_{L}^R by taking d to infinity in Eq. (22) before taking t to infinity [5,17]:

$$\frac{Z_{\mathrm{L}}^R}{\mathcal{L}} = \frac{Z_{\mathrm{non,sp}}(a)}{\mathcal{L}} + \frac{Z_{\mathrm{RW}}}{\mathcal{L}}, \tag{29}$$

where

$$\frac{Z_{\mathrm{non,sp}}(a)}{\mathcal{L}} = \frac{Z_{\mathrm{direct,sp}}}{\mathcal{L}} + \frac{Z_{\mathrm{indirect,sp}}}{\mathcal{L}}, \tag{30}$$

$$\frac{Z_{\mathrm{direct,sp}}}{\mathcal{L}} = -\frac{j2Z_0}{\bar{k}\pi\beta\gamma\sigma^2}\left(\frac{1}{2} - I_1(\bar{k}\sigma)K_1(\bar{k}\sigma)\right), \tag{31}$$

$$\frac{Z_{\mathrm{indirect,sp}}}{\mathcal{L}} = \frac{j2Z_0 K_0(\bar{k}a) I_1^2(\bar{k}\sigma)}{\bar{k}\pi\beta\gamma\sigma^2 I_0(\bar{k}a)}, \tag{32}$$

$$\frac{Z_{\mathrm{RW}}}{\mathcal{L}} = -\frac{j2Z_0 I_1^2(\bar{k}\sigma)}{\bar{k}\pi\beta\gamma\sigma^2}\left[\frac{K_0(\bar{k}a)}{I_0(\bar{k}a)} - \frac{K_0'(\bar{k}a)\left(1+\frac{jZ_0(\sigma_{2c}+j\omega\epsilon'\epsilon_0)K_0(\bar{k}a)K_0'(\nu_2 a)}{\nu_2\beta\gamma K_0'(\bar{k}a)K_0(\nu_2 a)}\right)}{I_0'(\bar{k}a)\left(1+\frac{jZ_0(\sigma_{2c}+j\omega\epsilon'\epsilon_0)I_0\left(\bar{k}a\right)K_0'(\nu_2 a)}{\beta\gamma\nu_2 I_0'\left(\bar{k}a\right)K_0(\nu_2 a)}\right)}\right]. \tag{33}$$

Equation (33) is rewritten as

$$\frac{Z_{\mathrm{RW}}}{\mathcal{L}} = \frac{Z_0\nu_2}{2\pi a I_0(a\bar{k})\left[\sigma_{2c}Z_0 I_0(\bar{k}a) + j\beta\gamma\nu_2 I_1(\bar{k}a)\right]}, \tag{34}$$

for an infinitesimal cylindrical beam ($\sigma = 0$). The prime on the modified Bessel functions $I_n(z)$ and $K_n(z)$ denotes the derivative with their argument z.

Because $Z_{\mathrm{RW}}/\mathcal{L}$ vanishes when σ_{2c} approaches infinity, the retained $Z_{\mathrm{non,sp}}(a)/\mathcal{L}$ represents the space charge impedance for the chamber with radius a including non-relativistic effects [23]. As a result, $Z_{\mathrm{direct,sp}}/\mathcal{L}$ describes the direct space charge impedance as $Z_{\mathrm{indirect,sp}}/\mathcal{L}$ approaches zero by taking a to infinity. In this way we can divide the direct-space-charge, indirect-space-charge, and resistive-wall impedances in Eqs. (20), (29), and (30).

The synchrotron tune is affected by the space charge impedance as well as the longitudinal resistive-wall impedance. We can deal with the space charge impedance with the perfectly conductive boundary and the resistive-wall impedance separately because the total impedance can be divided into them [21,26]. From a simulation standpoint, the particle-in-cell scheme (see, for example, Ref. [27]) is useful for evaluating the effect of the space charge effects with the bound-

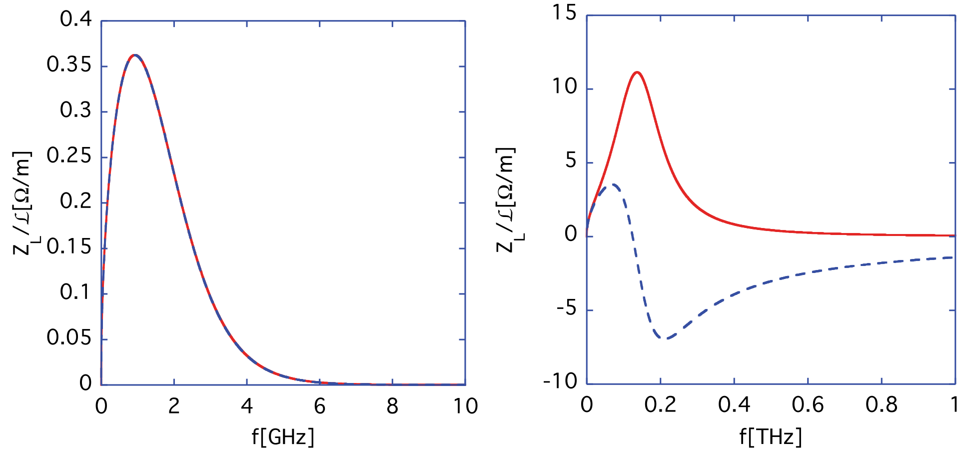

Fig. 5. Overall behavior of the longitudinal impedances for $\gamma = 2$ (left) and $\gamma = 10000$ (right), where $a = 65\,\text{mm}$, $\sigma_{2c} = 10^5\,\text{S}\,\text{m}^{-1}$, and $\epsilon' = \mu' = 1$. We symbolically represent Z_{L} on the vertical axis as the longitudinal impedance. The red solid and blue dashed lines denote the real and imaginary parts of the impedances, respectively.

ary condition on the tune, whereas the effect contributed by the resistive-wall impedance may be dealt with by implementing the impedance source along the accelerators [28].

In the case of an infinitesimal resistive chamber, the space charge impedance for a chamber with radius d can be reproduced as

$$\frac{Z_{\text{L}}^R}{\mathcal{L}} = -\frac{j2Z_0}{\bar{k}\pi\beta\gamma\sigma^2}\left(\frac{1}{2} - I_1(\bar{k}\sigma)K_1(\bar{k}\sigma)\right) + \frac{K_0\left(\bar{k}d\right)}{I_0\left(\bar{k}d\right)}\frac{2I_1^2\left(\bar{k}\sigma\right)jZ_0}{\bar{k}\sigma^2\beta\pi\gamma}, \tag{35}$$

by plugging $t = 0$ into Eq. (20).

Figure 5 depicts the overall behavior of the impedance $Z_{\text{RW}}/\mathcal{L}$ as calculated by Eq. (34). The longitudinal impedances for $\gamma = 2$ and $\gamma = 10\,000$ are shown in the left and the right panels, respectively. It is notable that the peak appears in the impedance's real part at [20]

$$f_R \simeq \frac{c}{\pi\left(\frac{\mu' a^2}{Z_0\sigma_c}\right)^{\frac{1}{3}}}, \tag{36}$$

for relativistic beams (right), where μ' is written explicitly differently from Ref. [20, Eq. (60)], but is well approximated to 1 at high frequency. This is because Eq. (34) is approximated for relativistic beams as

$$Z_{\text{RW}} \simeq \left[\frac{\sigma_{2c}2\pi a}{\sqrt{j\omega\mu_0\mu'\sigma_{2c}}\mathcal{L}} + j\omega\frac{\epsilon_0\pi a^2}{\mathcal{L}}\right]^{-1}, \tag{37}$$

where the first term with $\mu' = 1$ in the denominator represents the conventional resistive-wall admittance (Eq. (12)) and the second term represents the effective capacitance created by the chamber. Equation (36) explains the peak frequency f_R as 0.2 THz in the right panel of Fig. 5.

Comparing the left and right panels in Fig. 5 shows that as the beam becomes non-relativistic the peak frequency decreases, lowering the impedance. Because the slow beam receives more kicks from high-frequency radio-frequency (RF) fields while passing through the wake fields, the impedance tends to be suppressed toward high frequencies, resulting in a lower peak frequency.

However, if we focus on the lower-frequency part as $\bar{k}a \ll 1$, Eq. (34) is approximated as

$$\frac{Z_{\rm RW}}{\mathcal{L}} = \frac{Z_0\nu_2\left(1+\frac{j\beta\gamma\nu_2}{Z_0\sigma_{2c}}\right)}{2\pi a\left[\sigma_{2c}Z_0+\frac{j\beta\nu_2 ka}{2}+j\beta\gamma\nu_2-\frac{\beta^2\gamma\nu_2^2 ka}{2Z_0\sigma_{2c}}\right]}, \tag{38}$$

which is further simplified as

$$\frac{Z_{\rm L,non,RW}}{\mathcal{L}} \simeq \frac{\sqrt{j\omega\mu_0\mu'\sigma_{2c}}}{2a\pi\sigma_{2c}} + \frac{\omega^2\mu'}{4c^2\pi\sigma_{2c}}, \tag{39}$$

for a highly conductive chamber, regardless of whether the beam is relativistic or not. The conventional resistive-wall longitudinal impedance of Eq. (12) is represented by the first term in the case of $\mu' = 1$. The Lorentz-β dependence is noticeably absent at low frequency. This is because the longitudinal wakes excited by the beam behave as a cosine-line function and are nearly constant at low frequency during the beam passage [2,23].

3.2 *Impedance at low frequency for a chamber with finite thickness*

3.2.1 *Approximate formula for relativistic beams.* Let us now look at how the relativistic resistive-wall impedance vanishes for an extremely thin chamber and how it relates to the space charge impedance. We approximate Eq. (20) for relativistic beams with the parameter d kept finite by assuming the condition

$$\frac{\omega}{c\beta\gamma}d \ll 1. \tag{40}$$

Moreover, the Bessel functions are approximated as

$$I_n(z) \simeq \frac{e^z}{\sqrt{2\pi z}}, \qquad K_n(z) \simeq \sqrt{\frac{\pi}{2z}}e^{-z}, \tag{41}$$

for large arguments [24] by assuming highly conductive material, such as

$$|\nu_2(a+t)| \gg 1. \tag{42}$$

$|\nu_2(a+t)| \gg 1.$

In this case, at low frequencies the longitudinal impedance $Z_{\rm L}^R$ is expressed as

$$Z_{\rm L}^R = \frac{(1+j)R\tanh[(1+j)\frac{t}{\delta}]}{\sigma_{2c}a\delta} - \frac{j\omega RZ_0(a+t)\log\left[\frac{d}{(a+t)}\right]}{c\beta^2\gamma^2 a\cosh^2\left[(1+j)\frac{t}{\delta}\right]} - \frac{j\omega RZ_0}{2c\beta^2\gamma^2}g_f[a], \tag{43}$$

after $\mathcal{L} = 2\pi R$ is plugged in, where δ is again the skin depth:

$$\delta = \sqrt{\frac{2}{\mu'\mu_0\sigma_{2c}\omega}}, \tag{44}$$

and the g-factor, describing the space charge impedance of a cylindrical chamber with inner radius a for a cylindrical beam with radius σ, is given by

$$g_f[a] = \frac{1}{2} + 2\log\left[\frac{a}{\sigma}\right]. \tag{45}$$

Because we define the impedance as the average of the longitudinal electric field over the cross-section of the beam, following Ref. [1, Appendix 6.A], the constant term 1 in Eq. (17) is replaced by 1/2.

The final term of Eq. (43) depicts the conventional space charge impedance for a chamber with inner radius a. The first term reproduces the conventional resistive-wall impedance (Eq. (15)) for a finite-thickness t chamber in the case of $\mu' = 1$ [2]. Aside from that, the second term naturally appears, expressing the effect of fields filling the space between the inner and

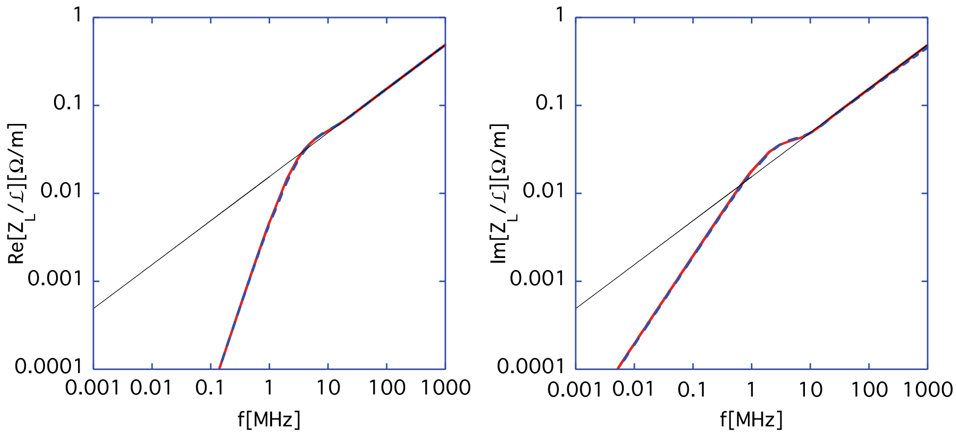

Fig. 6. Longitudinal impedances for $\gamma = 100$, where $\sigma = 5$ mm, $\sigma_{2c} = 10^5$ S m^{-1}, $a = 65$ mm, $d = 165$ mm, $t = 1$ mm, and $\epsilon^{'} = \mu^{'} = 1$. We symbolically represent Z_{L} on the vertical axis as the longitudinal impedance. The red solid, blue dashed, and black solid lines denote the impedances by Eq. (43), (46), and (12) respectively, where g is replaced by $\mathcal{L} = 2\pi R$.

outer chamber walls. When the thickness t reaches infinity the second term disappears, leaving only the resistive-wall impedance and the space-charge impedance for the chamber with inner radius a. For an infinitesimal thickness t, the total impedance produces the conventional relativistic space charge impedance for a chamber with inner radius d by combining the second and third terms as the resistive-wall impedance vanishes.

For small t, the real part of the resistive-wall impedance does not appear to produce DC resistance in the two-dimensional cylindrical chamber. Instead, as is already known, the resistive-wall impedance is vanishing. This is due to the fact that the wall-current begins to flow on the outermost chamber wall with radius d, which is more beneficial for minimizing the beam energy loss than continuing to flow on the inner thin chamber. In this sense, Eq. (43) for an ultra-relativistic beam may be approximated by a parallel electric circuit as follows:

$$Z_{\mathrm{L}}^{R} \simeq \left(\frac{1}{\frac{(1+j)R}{\sigma_{2c} a\delta \tanh\left[(1+j)\frac{t}{\delta}\right]} + \frac{j\omega R Z_0}{c\beta^2\gamma^2}\log\left[\frac{d}{a}\right]} + \frac{1}{R_{\mathrm{D}}} \right)^{-1} - \frac{j\omega R Z_0}{2c\beta^2\gamma^2}\left(\frac{1}{2} + 2\log\left[\frac{d}{\sigma}\right]\right), \tag{46}$$

with

$$R_{\mathrm{D}} = \frac{(1+j)R\sinh\left[2(1+j)\frac{t}{\delta}\right]}{\sigma_{2c}2a\delta}. \tag{47}$$

The dynamic resistance R_{D}, which describes the impedance of the vacuum between the inner and outer chambers and reaches zero for infinitesimal t while diverging for infinite t, appears in the denominator of the second term at low frequency.

The resistive-wall term and the difference in indirect space charge effects due to the inner and outer chambers are represented by the first and second terms in the denominator of the first term in Eq. (46). The final term represents the space charge impedance due to the chamber with the radius d.

Figure 6 shows a comparison of the longitudinal impedances calculated by Eq. (43) (red solid) and by Eq. (46) (blue dashed) for $\gamma = 100$. For reference, the black line denotes the conventional resistive-wall impedance with infinite thickness by Eq. (12), where g is replaced by $\mathcal{L} = 2\pi R$. The impedances deviate from the conventional formula for $\delta > t = (1\,\mathrm{mm})$ ($f < 2.5$ MHz in this case). Although the first term in the denominator of the first term in Eq. (46) produces the

DC resistance for infinitesimal t (compare it to the second term in the admittance in Eq.(3)), Eq. (46) based on the parallel circuit model approximates the original impedance by Eq. (43) well. As a result, Eq. (46) generates the space charge impedance for the chamber with radius d for infinitesimal t, while it generates the resistive-wall impedance in conjunction with the space charge impedance for the chamber with radius a for infinite t.

Another issue appears to arise in this case, because the conventional relativistic space charge impedance for the outermost chamber with inner radius d, expressed as

$$Z_{\mathrm{L}}^{R} = -\frac{j\omega R Z_0}{2c\beta^2\gamma^2}\left(\frac{1}{2} + 2\log\left[\frac{d}{\sigma}\right]\right), \tag{48}$$

becomes infinite as d approaches infinity. In principle, however, only the direct space charge impedance (Eq. (31)) should be retained for the limit. This discrepancy can be reconciled by understanding how the approximate formula in Eq. (43) is derived from the rigorous formula, Eq. (20). We use the condition in Eq. (40) in the derivation. As a result, the parameter d in Eqs. (43), (46), and (48) cannot be infinite, because they must be used under the condition in Eq. (40).

3.2.2 *Relation to the DC resistance in the previous resistive-wall impedance of a two-dimensional cylindrical chamber.* Let us examine how the impedance behaves for a very thin wall with $t \ll \delta$ and whether the DC resistance of the chamber can play a significant role in the longitudinal impedance, because Ref. [1, Appendix 6.A] explains that DC resistance is reproduced under a condition.

The parameter d is set to be infinite from the start in Ref. [1, Appendix 6.A]. Therefore, let us take the limit in Eq. (20) as d approaches infinity, so that the last terms in Eqs. (23) and (24) vanish as they are proportional to $K_0(\bar{k}d)/I_0(\bar{k}d)$.

We can use Eq. (41) for large arguments for the highly conductive chamber given by Eq. (42), and the longitudinal impedance at low frequency is approximated as

$$Z_{\mathrm{L}}^{R} = kRZ_0\left[-\frac{jg_f[a]}{2\beta\gamma^2} + j\mu'\beta\left(\frac{t\left(1+\frac{\left(1+\Gamma+\log\left[\frac{ak}{2\gamma}\right]\right)}{\mu'\beta^2\gamma^2}\right)}{a} + \frac{\left(\Gamma+\log\left[\frac{ka}{2\gamma}\right]\right)}{\mu'\beta^2\gamma^2}\right)\right.$$
$$\left. + 2a\beta\mu' t\left(\sqrt{\frac{\omega\mu'\mu_0\sigma_{2c}}{2}}\right)^2\left(\frac{\Gamma+\log\left[\frac{ka}{2\gamma}\right]}{\mu'\beta^2\gamma^2}\right)^2\right], \tag{49}$$

for ultra-relativistic beams, which is equivalent to Ref. [1, Eq. (6.113)], where Γ is the Euler Γ, though the original Eq. (6.113) contains a typo. In the case of $t = 0$, Eq. (49) reproduces the direct space charge impedance

$$Z_{\mathrm{L}}^{R} = -\frac{jkRZ_0}{2\beta\gamma^2}\left(\frac{1}{2} + 2\log\left[\frac{1}{\frac{\bar{k}\sigma}{2}}\right] - 2\Gamma\right), \tag{50}$$

in Ref. [1, Appendix 6.A], which is equivalent to the rigorous formula in Eq. (31) for the direct space charge impedance after the approximation

$$\frac{\omega\sigma}{c\beta\gamma} \ll 1, \tag{51}$$

is applied.

To reproduce Ref. [1, Eq. (6.114)], describing the longitudinal impedance with the parallel circuit model, we must first assume the condition

$$1 \gg \frac{1+\Gamma+\log\left[\frac{ak}{2\gamma}\right]}{\mu'\beta^2\gamma^2}, \tag{52}$$

so that Eq. (49) is rewritten as

$$Z_{\mathrm{L}}^R = -\frac{jkRZ_0 g_f[a]}{2\beta\gamma^2} + \frac{1}{\mathcal{R}_e{}^{-1}+\mathcal{I}_e{}^{-1}}, \tag{53}$$

where

$$\mathcal{R}_e = \frac{kRZ_0\mu'\beta\left(\frac{t}{a}+\frac{\left(\Gamma+\log\left[\frac{ka}{2\gamma}\right]\right)}{\mu'\beta^2\gamma^2}\right)^2}{2at\left(\sqrt{\frac{\omega\mu'\mu_0\sigma_{2c}}{2}}\right)^2\left(\frac{\Gamma+\log\left[\frac{ka}{2\gamma}\right]}{\mu'\beta^2\gamma^2}\right)^2}\left[1+\frac{4a^2t^2\left(\sqrt{\frac{\omega\mu'\mu_0\sigma_{2c}}{2}}\right)^4\left(\frac{\Gamma+\log\left[\frac{ka}{2\gamma}\right]}{\mu'\beta^2\gamma^2}\right)^4}{\left(\frac{t}{a}+\frac{\left(\Gamma+\log\left[\frac{ka}{2\gamma}\right]\right)}{\mu'\beta^2\gamma^2}\right)^2}\right], \tag{54}$$

$$\mathcal{I}_e = j\frac{kRZ_0\mu'\beta\left(\frac{t}{a}+\frac{\left(\Gamma+\log\left[\frac{ka}{2\gamma}\right]\right)}{\mu'\beta^2\gamma^2}\right)^2}{\left(\frac{t}{a}+\frac{\left(\Gamma+\log\left[\frac{ka}{2\gamma}\right]\right)}{\mu'\beta^2\gamma^2}\right)}\left[1+\frac{4a^2t^2\left(\sqrt{\frac{\omega\mu'\mu_0\sigma_{2c}}{2}}\right)^4\left(\frac{\Gamma+\log\left[\frac{ka}{2\gamma}\right]}{\mu'\beta^2\gamma^2}\right)^4}{\left(\frac{t}{a}+\frac{\left(\Gamma+\log\left[\frac{ka}{2\gamma}\right]\right)}{\mu'\beta^2\gamma^2}\right)^2}\right]. \tag{55}$$

Here, when the conditions

$$\frac{t}{a} \ll \frac{\left(\Gamma+\log\left[\frac{ka}{2\gamma}\right]\right)}{\mu'\beta^2\gamma^2}, \tag{56}$$

$$4a^2t^2\left(\sqrt{\frac{\omega\mu'\mu_0\sigma_{2c}}{2}}\right)^4\left(\frac{\Gamma+\log\left[\frac{ka}{2\gamma}\right]}{\mu'\beta^2\gamma^2}\right)^4 \ll \left(\frac{t}{a}+\frac{\left(\Gamma+\log\left[\frac{ka}{2\gamma}\right]\right)}{\mu'\beta^2\gamma^2}\right)^2, \tag{57}$$

are satisfied, Eqs. (54) and (55) can be approximated as

$$\mathcal{R}_e \simeq \frac{R}{at\sigma_{2c}}\left[1+2\frac{t}{a\left(\frac{\Gamma+\log\left[\frac{ka}{2\gamma}\right]}{\mu'\beta^2\gamma^2}\right)}\right], \tag{58}$$

$$\mathcal{I}_e \simeq j\omega R\mu_0\frac{\left(\Gamma+\log\left[\frac{ka}{2\gamma}\right]\right)}{\beta^2\gamma^2}\left[1+\frac{t}{a\left(\frac{\Gamma+\log\left[\frac{ka}{2\gamma}\right]}{\mu'\beta^2\gamma^2}\right)}\right], \tag{59}$$

removing the typo of Ref. [1, Eq. (6.115)]. As a result, the resistive-wall longitudinal impedance with relativistic beams for a very thin wall with $t \ll \delta$ in Ref. [1, Appendix 6.A] is summarized as

$$\frac{Z_L^R}{R} = -j\omega\frac{\mu_0\left(\frac{1}{2}+2\log\left[\frac{a}{\sigma}\right]\right)}{2\beta^2\gamma^2}$$
$$+\left\{\frac{1}{\frac{1}{at\sigma_{2c}}\left[1+2\frac{t}{a\left(\frac{\Gamma+\log\left[\frac{ka}{2\gamma}\right]}{\mu'\beta^2\gamma^2}\right)}\right]}+\frac{1}{j\omega\frac{\mu_0}{\beta^2\gamma^2}\left(\Gamma+\log\left[\frac{ka}{2\gamma}\right]\right)\left[1+\frac{t}{a\left(\frac{\Gamma+\log\left[\frac{ka}{2\gamma}\right]}{\mu'\beta^2\gamma^2}\right)}\right]}\right\}^{-1}, \quad (60)$$

after Eqs. (58) and (59) are substituted into Eq. (53).

As Ref. [1, Appendix 6.A] suggests, the first term in Eq. (58) represents the DC resistance of the chamber; however, when the DC resistance plays a significant role in Eq. (53) (or Eq. (60)), the condition $\mathcal{R}_e \ll \mathcal{I}_e$, which is

$$\frac{1}{\sigma_{2c}at} \ll \omega\mu_0\frac{\left(\Gamma+\log\left[\frac{ka}{2\gamma}\right]\right)}{\beta^2\gamma^2}, \quad (61)$$

occurs, referring to Eqs. (58) and (59).

However, the condition in Eq. (57) is simplified as

$$\sigma_{2c}at\omega\mu_0\frac{\left(\Gamma+\log\left[\frac{ka}{2\gamma}\right]\right)}{\beta^2\gamma^2} \ll 1, \quad (62)$$

using Eq. (56), which contradicts the condition in Eq. (61). Consequently, the DC resistance cannot emerge in the impedance under any circumstances, which can be easily found in the original formula, Eq. (49).

Figure 7 shows one example calculated by Eq. (60), where $\gamma = 1000$, $\sigma = 10$ mm, $\sigma_{2c} = 10^5$ S m^{-1}, $a = 65$ mm, $t = 1$ mm, and $\epsilon' = \mu' = 1$. Apparently, there is no region where the real part of the impedance becomes DC resistance in $t < \delta$ (i.e. $f < 2.53$ MHz). Moreover,

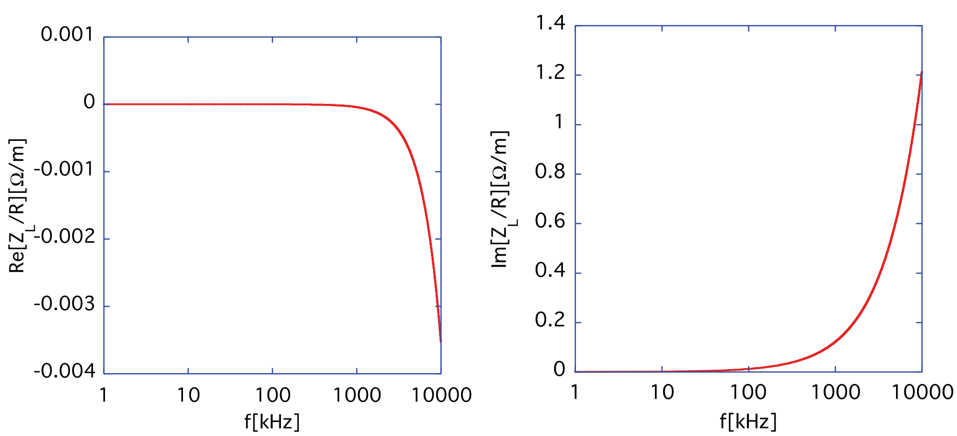

Fig. 7. Longitudinal impedance calculated by Eq. (60), where $\gamma = 1000$, $\sigma = 10$ mm, $\sigma_{2c} = 10^5$ S m^{-1}, $a =$ 65 mm, $t = 1$ mm, and $\epsilon' = \mu' = 1$. We symbolically represent Z_L on the vertical axis as the longitudinal impedance.

the real part of the impedance is negative, being unphysical, though the imaginary part of the impedance is inductive. Finally, we conclude that Eq. (60) (or Ref. [1, Eq. (6.114)]) is not a suitable expression for the longitudinal impedance at low frequency for relativistic beams.

3.2.3 *Approximate formula for non-relativistic beams.* In this section we will look at the resistive-wall impedance of a chamber with a finite thickness that is applicable to non-relavisitic beams. Equation (20) is approximated well for the highly conductive chamber as

$$\frac{Z_{\mathrm{L}}^R}{\mathcal{L}} \simeq \frac{Z_{\mathrm{non,sp}}(a)}{\mathcal{L}} + \frac{Z_{\mathrm{non,res}}}{\mathcal{L}}, \tag{63}$$

where

$$\begin{aligned}\frac{Z_{\mathrm{non,res}}}{\mathcal{L}} = -\Bigg[& \frac{j2Z_0 I_1^2(\bar{k}\sigma)\left\{K_0(\bar{k}(a+t)) - \frac{K_0(\bar{k}d)I_0(\bar{k}(a+t))}{I_0(\bar{k}d)} + \frac{j\beta\gamma\nu_2\left[K_1(\bar{k}(a+t)) + \frac{K_0(\bar{k}d)I_1(\bar{k}(a+t))}{I_0(\bar{k}d)}\right]\tanh\nu_2 t}{Z_0\sigma_{2c}}\right\}}{\bar{k}^2\sigma^2 a\beta\pi\gamma I_0(\bar{k}a)(I_0(\bar{k}a)K_1(\bar{k}(a+t)) + I_1(\bar{k}a)K_0(\bar{k}(a+t)))\tanh\nu_2 t}\Bigg] \\ & \times\Bigg[\frac{1}{\tanh\nu_2 t} + \frac{\frac{\sigma_{2c}^2 Z_0^2 I_0(\bar{k}a)K_0(\bar{k}(a+t)) - \beta^2\gamma^2\nu_2^2 I_1(\bar{k}a)K_1(\bar{k}(a+t))}{j\beta\gamma\nu_2 Z_0\sigma_{2c}}}{(I_0(\bar{k}a)K_1(\bar{k}(a+t)) + I_1(\bar{k}a)K_0(\bar{k}(a+t)))} \\ & - \frac{\frac{K_0(\bar{k}d)[Z_0^2\sigma_{2c}^2 I_0(\bar{k}a)I_0(\bar{k}(a+t)) + \beta^2\gamma^2\nu_2^2 I_1(\bar{k}a)I_1(\bar{k}(a+t))]}{j\beta\gamma\nu_2 Z_0\sigma_{2c}I_0(\bar{k}d)}}{(I_0(\bar{k}a)K_1(\bar{k}(a+t)) + I_1(\bar{k}a)K_0(\bar{k}(a+t)))}\Bigg]^{-1},\end{aligned} \tag{64}$$

following the application of Eq. (41). Equation (63) goes to the non-relativistic space charge impedance $Z_{\mathrm{non,sp}}(d)/\mathcal{L}$ of the chamber with radius d for infinitesimal t, while it reproduces Eq. (34) for the resistive-wall impedance with the space charge impedance of $Z_{\mathrm{non,sp}}(a)/\mathcal{L}$ by taking d and t to infinity. Equation (43) is thus generalized to Eq. (63), which can deal with non-relativistic beams as well.

Figure 8 compares the rigorous result of the longitudinal resistive-wall impedances by Eq. (22) (red), approximate results by Eq. (64) (blue dashed), and the conventional formula in Eq. (12) (black dashed) with infinite thickness, where g is replaced by $\mathcal{L}$. The upper and lower panels show the outcomes for $\gamma = 2$ and $\gamma = 1000$, respectively. Regardless of whether the beam is relativistic or not, the longitudinal impedance calculated by Eq. (64) is nearly identical to the rigorous result calculated using Eq. (22). Both results deviate from the conventional formula in Eq. (12) for $\delta > t$, i.e. $f < 2.5$ MHz. The real part of the impedance for $\gamma = 2$ clearly defines the frequency region where the impedance becomes DC resistance in $\delta > t$, even though the impedance reaches zero at the frequency origin even in this case.

The phenomenon is comprehended in the same way as in the relativistic case, as follows. At low frequencies such as

$$\frac{2\pi f d}{c\beta\gamma} \ll 1, \tag{65}$$

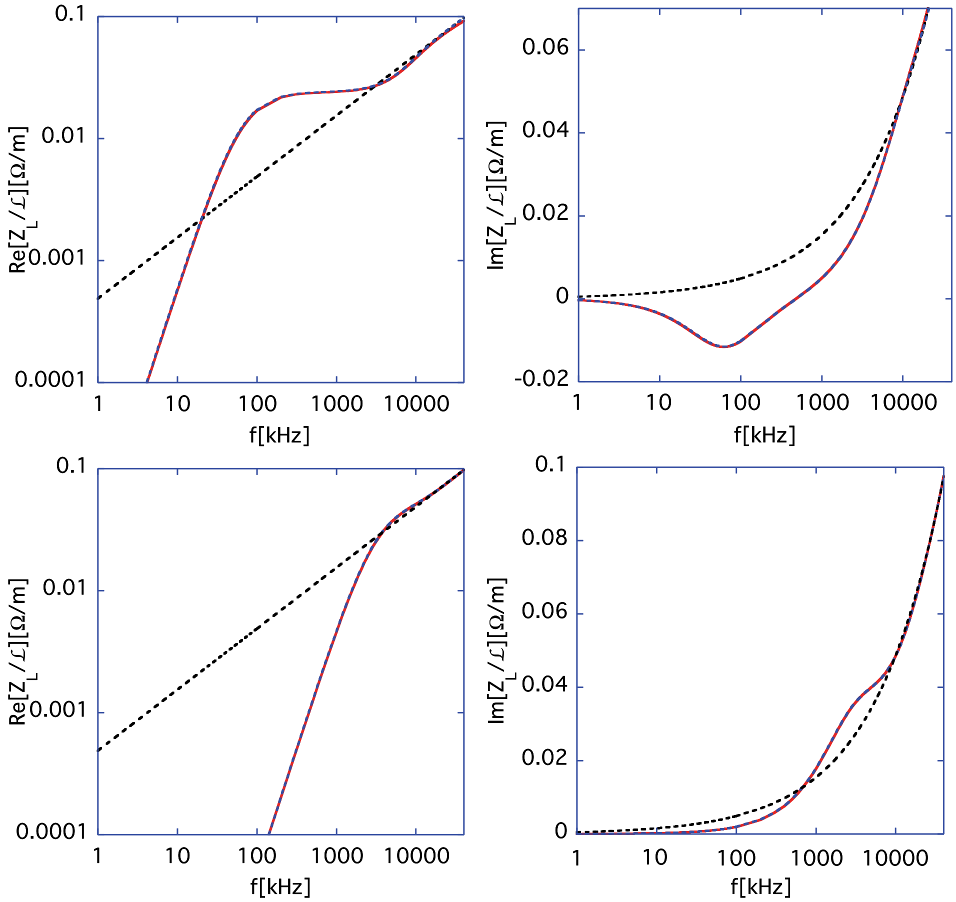

Fig. 8. Longitudinal resistive-wall impedances except the space charge impedance for $\gamma = 2$ (upper) and $\gamma = 1000$ (lower), where $\sigma = 10\,\mathrm{mm}$, $\sigma_{2c} = 10^5\,\mathrm{S\,m^{-1}}$, $a = 65\,\mathrm{mm}$, $d = 165\,\mathrm{mm}$, $t = 1\,\mathrm{mm}$, and $\epsilon' = \mu' = 1$. We symbolically represent Z_{L} on the vertical axis as the longitudinal impedance. The red solid, blue dashed, and black dashed lines denote the impedances calculated by Eqs. (22), (64), and (12) respectively, where g is replaced by $\mathcal{L}$.

Eq. (64) is approximated as

$$\frac{Z_{\mathrm{L}}^R}{\mathcal{L}} \simeq -\frac{jkZ_0\left(\frac{1}{2}+2\log\left[\frac{a}{\sigma}\right]\right)}{4\pi\beta\gamma^2} + \frac{\nu_2\left(j\beta\gamma^2\nu_2\tanh(\nu_2 t)+k(a+t)Z_0\sigma_{2c}\log\left[\frac{d}{(a+t)}\right]\right)}{2a\pi\sigma_{2c}\left(j\beta\gamma^2\nu_2+k(a+t)Z_0\sigma_{2c}\log\left[\frac{d}{(a+t)}\right]\tanh(\nu_2 t)\right)}, \tag{66}$$

where the first term represents the space charge impedance for the chamber with radius a. When t is set to zero, Eq. (66) reproduces the space charge impedance for the chamber with radius d. When the ultra-relativistic beam passes through the resistive chamber with $\mu' = 1$, Eq. (66) is identical to the conventional formula, Eq. (15), of the resistive-wall impedance with finite thickness including the conventional space charge impedance for the chamber with radius a, but it becomes

$$\frac{Z_{\mathrm{L}}^R}{\mathcal{L}} \simeq -\frac{jkZ_0\left(\frac{1}{2}+2\log\left[\frac{a}{\sigma}\right]\right)}{4\pi\beta\gamma^2} + \frac{\nu_2}{2a\pi\sigma_{2c}\tanh(\nu_2 t)}, \tag{67}$$

for the highly conductive chamber with non-relativistic beams in the frequency range

$$\frac{c\beta^2\gamma^2}{2\pi t\sigma_{2c}\sqrt{(a+t)Z_0^2\log\left[\frac{d}{(a+t)}\right]\left(-t\beta^2\gamma^2\mu'+(a+t)\log\left[\frac{d}{(a+t)}\right]\right)}}<f<\frac{c}{\pi t^2 Z_0\mu'\sigma_{2c}}. \quad (68)$$

The flat region from 60 kHz to 2500 kHz in the upper-left panel of Fig. 8 is well explained by the inequality relation in Eq. (68). The second term of Eq. (67) reproduces the DC resistance for infinitesimal t.

To investigate the characteristic, let us rewrite Eq. (66) using the parallel circuit model. In the case of $t \ll a$, Eq. (66) is approximated as

$$\frac{Z_L^R}{\mathcal{L}}\simeq-\frac{j\omega Z_0\left(\frac{1}{2}+2\log\left[\frac{d}{\sigma}\right]\right)}{4\pi c\beta^2\gamma^2}+\left[\frac{1}{\left(\frac{(1+j)}{2\pi a\sigma_{2c}\delta\tanh\left[(1+j)\frac{t}{\delta}\right]}+\frac{j\omega Z_0\log\left[\frac{d}{a}\right]}{2\pi c\beta^2\gamma^2}\right)}+\frac{1}{Z_2}\right]^{-1}, \quad (69)$$

where

$$Z_2=\left[\frac{(1+j)}{4\pi a\sigma_{2c}\delta}+\frac{j\omega Z_0\tanh\left(\frac{(1+j)t}{\delta}\right)\log\left[\frac{d}{a}\right]}{4\pi c\beta^2\gamma^2}\right]\left[1+\frac{j\omega a(a+t)Z_0\sigma_{2c}\log\left[\frac{d}{(a+t)}\right]\log\left[\frac{a}{d}\right]}{c\beta^4\gamma^4\mu'}\right]$$
$$\times\ \sinh\left(\frac{2(1+j)t}{\delta}\right). \quad (70)$$

In this case, the dynamic resistance R_D in Eq. (47), which describes the vacuum impedance between the inner and outer chambers, is generalized to the Lorentz-γ-dependent impedance Z_2 in Eq. (70). As the beam becomes ultra-relativistic, the impedance Z_2 approaches zero faster for a very thin chamber with $t = 0$, resulting in the space charge impedance of a chamber with radius d in Eq. (69). In other words, the impedance Z_2 for the non-relativistic beams could become high, because of the high conductivity σ_{2c} (see the second term in the second bracket in Eq. (70)). As a result, the DC resistance (the first term with $t \ll \delta$ in the first denominator of the second term in Eq. (69)) plays a significant role in Eq. (69) for non-relativistic beams, which is not the case for relativistic beams.

Figure 9 contrasts the longitudinal impedances calculated by Eqs. (63) and (69). The blue dashed and red solid lines denote the impedances from Eqs. (63) and (69), respectively. The upper and lower panels represent the results for $\gamma = 2$ and $\gamma = 1000$ respectively, including the space charge impedance. The parameters used are identical to those in Fig. 8. Figure 9 demonstrates that Eq. (69) based on the parallel circuit model approximates well Eq. (63) in the frequency range below 1 GHz in this example.

The condition in Eq. (68) suggests that the Lorentz γ has the upper limit

$$\gamma^2<1+\frac{2(\sqrt{2}-1)(a+t)\log\left[\frac{d}{(a+t)}\right]}{t\mu'}, \quad (71)$$

to ensure the appearance of DC resistance in the impedance, indicating that increasing d appears to broaden the frequency range where DC resistance emerges, regardless of whether the beam is relativistic or not. The condition in Eq. (65), on the other hand, imposes an upper limit on d. Using the condition $\delta > t$ in conjunction with Eq. (65), we obtain

$$d \ll \frac{\beta\gamma\pi t^2 Z_0\mu'\sigma_{2c}}{2\pi}. \quad (72)$$

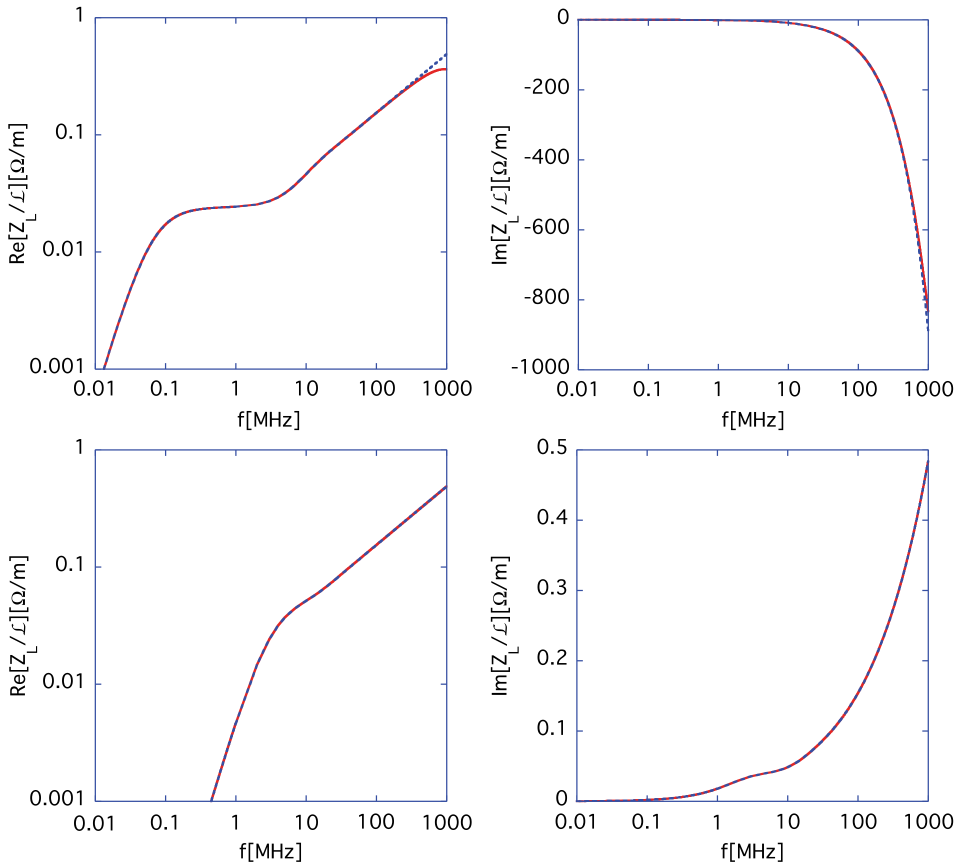

Fig. 9. Longitudinal impedances for $\gamma = 2$ (upper) and $\gamma = 1000$ (lower), including the space charge impedance, where $\sigma = 10\,\text{mm}$, $\sigma_{2c} = 10^5\,\text{S m}^{-1}$, $a = 65\,\text{mm}$, $d = 165\,\text{mm}$, $t = 1\,\text{mm}$, and $\epsilon' = \mu' = 1$. We symbolically represent Z_L on the vertical axis as the longitudinal impedance. The blue dashed and red solid lines denote the impedances from Eqs. (63) and (69), respectively.

When Eqs. (71) and (72) are combined, the following conclusion is obtained:

$$d \ll \frac{\pi t^2 Z_0 \mu' \sigma_{2c}}{2\pi} \sqrt{\frac{2(\sqrt{2}-1)(a+t)\log\left[\frac{d}{(a+t)}\right]}{t\mu'}}, \tag{73}$$

which can be easily broken by increasing d. Again, it becomes more difficult to create a DC resistance region in the longitudinal impedance toward relativistic beams.

To consider the case where d is infinite, we must make d infinite while keeping t finite in Eq. (64) from the start, rather than using Eq. (66) owing to the condition in Eq. (65). The impedance is denoted as

$$\frac{Z_\text{L}^R}{\mathcal{L}} = \frac{Z_{\text{non,sp}}(a)}{\mathcal{L}} - \left\{ \frac{j2Z_0 I_1^2(\bar{k}\sigma)\left[K_0(\bar{k}(a+t)) + \frac{j\beta\gamma\nu_2 K_1(\bar{k}(a+t))\tanh\nu_2 t}{Z_0\sigma_{2c}}\right]}{\bar{k}^2\sigma^2 a\beta\pi\gamma I_0(\bar{k}a)(I_0(\bar{k}a)K_1(\bar{k}(a+t)) + I_1(\bar{k}a)K_0(\bar{k}(a+t)))} \right\}$$
$$\times \left\{ 1 + \frac{\left[\frac{\sigma_{2c}^2 Z_0^2 I_0(\bar{k}a)K_0(\bar{k}(a+t)) - \beta^2\gamma^2\nu_2^2 I_1(\bar{k}a)K_1(\bar{k}(a+t))}{j\beta\gamma\nu_2 Z_0\sigma_{2c}}\right]\tanh\nu_2 t}{(I_0(\bar{k}a)K_1(\bar{k}(a+t)) + I_1(\bar{k}a)K_0(\bar{k}(a+t)))} \right\}^{-1}, \tag{74}$$

which is approximated at low frequency ($\bar{k}(a+t) \ll 1$) as

$$\frac{Z_{\rm L}^R}{\mathcal{L}} \simeq -\frac{jkZ_0\left(\frac{1}{2}+2\log\left[\frac{a}{\sigma}\right]\right)}{4\pi\beta\gamma^2} + \frac{\nu_2\left[j\beta\gamma^2\nu_2\tanh(t\nu_2)+k(a+t)Z_0\sigma_{2c}\left(-\Gamma-\log\left[\frac{k(a+t)}{2\gamma}\right]\right)\right]}{2a\pi\sigma_{2c}\left\{j\beta\gamma^2\nu_2+k(a+t)Z_0\sigma_{2c}\left(-\Gamma-\log\left[\frac{k(a+t)}{2\gamma}\right]\right)\tanh(t\nu_2)\right\}}, \tag{75}$$

while Eq. (34) should be applied where the skin depth is less than the chamber thickness t at high frequency.

Equation (75) is further approximated as

$$\frac{Z_{\rm L}^R}{\mathcal{L}} \simeq -\frac{jkZ_0\left(\frac{1}{2}+2\log\left[\frac{a}{\sigma}\right]\right)}{4\pi\beta\gamma^2} + \frac{(1+j)\tanh\left((1+j)\frac{t}{\delta}\right)}{2a\pi\sigma_{2c}\delta}, \tag{76}$$

reproducing the simple summation of the very conventional resistive-wall impedance formula in Eq. (15) and the space charge impedance after $\mu^{'}=1$ is plugged into Eq. (76) for relativistic beams, as already seen in Sect. 2.

For the highly conductive chamber with non-relativistic beams, Eq. (75) is approximated as

$$\frac{Z_{\rm L}^R}{\mathcal{L}} \simeq -\frac{jkZ_0\left(\frac{1}{2}+2\log\left[\frac{a}{\sigma}\right]\right)}{4\pi\beta\gamma^2} + \frac{\nu_2}{2a\pi\sigma_{2c}\tanh(\nu_2 t)}, \tag{77}$$

for

$$f_{\rm b} \lesssim f < \frac{c}{\pi t^2 Z_0\mu'\sigma_{2c}}, \tag{78}$$

and

$$\frac{Z_{\rm L}^R}{\mathcal{L}} \simeq -\frac{jkZ_0\left(\frac{1}{2}+2\log\left[\frac{a}{\sigma}\right]\right)}{4\pi\beta\gamma^2} + \frac{kZ_0\left(a\Gamma+t(\Gamma+\beta^2\gamma^2\mu')+(a+t)\log\left[\frac{(k(a+t))}{2\gamma}\right]\right)}{2a\pi\left(-j\beta\gamma^2+\Gamma kt(a+t)Z_0\sigma_{2c}+kt(a+t)Z_0\sigma_{2c}\log\left[\frac{(k(a+t))}{2\gamma}\right]\right)}, \tag{79}$$

for $0 \le f < f_{\rm b}$, where

$$f_{\rm b} = \frac{c\beta^2\gamma^2}{2\pi t\sigma_{2c}Z_0\sqrt{(a+t)\left(\Gamma+\log\left[\frac{(a+t)}{t^2\beta\gamma\mu' Z_0\sigma_{2c}}\right]\right)\left(t\beta^2\gamma^2\mu'+(a+t)\left(\Gamma+\log\left[\frac{(a+t)}{t^2\beta\gamma\mu' Z_0\sigma_{2c}}\right]\right)\right)}}. \tag{80}$$

Particularly for infinitesimal t, Eqs. (75) and (79) reproduce the direct space charge impedance as Eq. (50), while the second term in Eq. (77) represents the DC resistance.

Figure 10 compares the longitudinal impedance calculated using Eq. (74) (blue dashed) to that by Eq. (75) (red solid), but only for the non-relativistic case ($\gamma = 2$), where the the space charge impedance is included and the parameters are the same as in Fig. 9. Equation (75) accurately approximates the results of Eq. (74) at low frequency. We can identify the DC resistance in the left panel of Fig. 10. The frequency range estimated as $f_u = 9$ kHz to 2.5 MHz by Eq. (78) is wider than that in the upper-left panel of Fig. 9 because the wall-current tries to continue flowing in the resistive chamber rather than the imaginary perfectly conductive chamber at a very far distance.

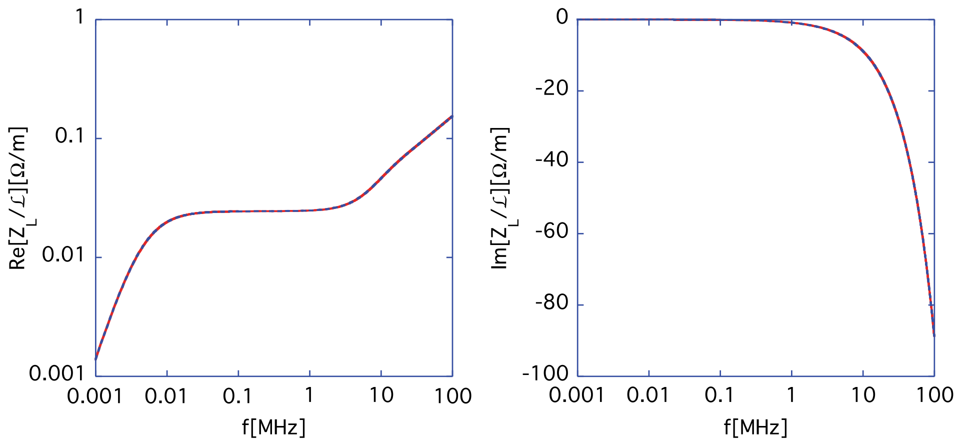

Fig. 10. Longitudinal impedances for $\gamma = 2$ with space charge impedance, where $\sigma = 10\,\mathrm{mm}$, $\sigma_{2c} = 10^5\,\mathrm{S\,m^{-1}}$, $a = 65\,\mathrm{mm}$, $t = 1\,\mathrm{mm}$, and $\epsilon^{'} = \mu^{'} = 1$. We symbolically represent Z_{L} on the vertical axis as the longitudinal impedance. The impedances calculated by Eqs. (74) and (75) are respectively denoted by the blue dashed and red solid lines.

4. Transverse resistive-wall impedance of a two-dimensional cylindrical chamber

4.1 *Overview and rigorous formula for the transverse resistive-wall impedance*

As in the case of longitudinal impedance discussed in Sect. 3, consider an infinitely thick perfectly conductive chamber with radius d outside the resistive chamber with inner radius a and thickness t (refer to Fig. 4). Equation (A52) in the appendix provides the rigorous formula for the transverse impedance Z_{T}, which includes the non-relativistic transverse space charge impedance per unit length [23,29],

$$Z_{\mathrm{non,sp,T}}[a] = \frac{kZ_0}{j2\pi r_{\mathrm{b}}\beta\gamma^3}\left[K_1(\bar{k}r_{\mathrm{b}}) - I_1(\bar{k}r_{\mathrm{b}})\frac{K_1(\bar{k}a)}{I_1(\bar{k}a)}\right], \tag{81}$$

for the chamber with radius a by solving Maxwell equations (refer to Sects. A1 and A3 in the appendix).

The total transverse impedance Z_{T} is denoted as

$$\frac{Z_{\mathrm{T}}}{\mathcal{L}} = -\frac{A(k)}{2c\beta\gamma} + \frac{kZ_0K_1(\bar{k}r_{\mathrm{b}})}{j2\pi r_{\mathrm{b}}\beta\gamma^3}, \tag{82}$$

with

$$A(k) = \frac{S_{22}b_1 - S_{12}b_2}{S_{11}S_{22} - S_{12}S_{21}}, \tag{83}$$

where the second term in Eq. (82) denotes the direct transverse space charge impedance,

$$
\begin{aligned}
S_{11} = {} & \frac{\gamma\beta k\nu_2^3(a+t)a\left[\frac{j\gamma\beta\nu_2 I_1'(\bar{k}a)\mathcal{F}_1(\nu_2 a)}{Z_0(\sigma_{2c}+j\omega\epsilon_0\epsilon')} - I_1\left(\bar{k}a\right)\mathcal{F}_3(\nu_2 a)\right]\left[K_1'\left(\bar{k}(a+t)\right) - \frac{K_1\left(\bar{k}d\right)I_1'\left(\bar{k}(a+t)\right)}{I_1\left(\bar{k}d\right)}\right]}{Z_0(\nu_2^2\gamma^2-k^2)\left[K_1\left(\bar{k}(a+t)\right) - \frac{K_1'\left(\bar{k}d\right)I_1\left(\bar{k}(a+t)\right)}{I_1'\left(\bar{k}d\right)}\right]\left[K_1\left(\bar{k}(a+t)\right) - \frac{K_1\left(\bar{k}d\right)I_1\left(\bar{k}(a+t)\right)}{I_1\left(\bar{k}d\right)}\right]} \\
& + \frac{\left(\frac{\nu_2^2\gamma^2}{k^2}-1\right)\mathcal{F}_1(\nu_2 a)I_1(\bar{k}a)}{\beta Z_0\mu'\left[K_1\left(\bar{k}(a+t)\right) - \frac{K_1'\left(\bar{k}d\right)I_1\left(\bar{k}(a+t)\right)}{I_1'\left(\bar{k}d\right)}\right]} \\
& - \frac{k\nu_2^2 a(a+t)\left[\frac{\nu_2\beta\gamma I_1'(\bar{k}a)\mathcal{F}_2(\nu_2 a)}{Z_0} + j(\sigma_{2c}+j\omega\epsilon_0\epsilon')I_1\left(\bar{k}a\right)F_4(\nu_2 a)\right]}{(\nu_2^2\gamma^2-k^2)\left[K_1\left(\bar{k}(a+t)\right) - \frac{K_1'\left(\bar{k}d\right)I_1\left(\bar{k}(a+t)\right)}{I_1'\left(\bar{k}d\right)}\right]},
\end{aligned} \tag{84}
$$

$$
\begin{aligned}
S_{22} = {} & \frac{\beta\gamma Z_0\nu_2^3(a+t)a\left[-\frac{\gamma\nu_2\mathcal{F}_1(\nu_2 a)I_1'(\bar{k}a)}{\mu'} + k\mathcal{F}_3(\nu_2 a)I_1\left(\bar{k}a\right)\right]\left[K_1'\left(\bar{k}(a+t)\right) - \frac{K_1'\left(\bar{k}d\right)I_1'\left(\bar{k}(a+t)\right)}{I_1'\left(\bar{k}d\right)}\right]}{(\nu_2^2\gamma^2-k^2)\left[K_1\left(\bar{k}(a+t)\right) - \frac{K_1\left(\bar{k}d\right)I_1\left(\bar{k}(a+t)\right)}{I_1\left(\bar{k}d\right)}\right]\left[K_1\left(\bar{k}(a+t)\right) - \frac{K_1'\left(\bar{k}d\right)I_1\left(\bar{k}(a+t)\right)}{I_1'\left(\bar{k}d\right)}\right]} \\
& - \frac{jk\left(\frac{\nu_2^2\gamma^2}{k^2}-1\right)\mathcal{F}_1(\nu_2 a)I_1(\bar{k}a)}{(\sigma_{2c}+j\omega\epsilon_0\epsilon')\left[K_1\left(\bar{k}(a+t)\right) - \frac{K_1\left(\bar{k}d\right)I_1\left(\bar{k}(a+t)\right)}{I_1\left(\bar{k}d\right)}\right]} \\
& + \frac{\nu_2^2 k\beta(a+t)aZ_0\left[-k\mu'\mathcal{F}_4(\nu_2 a)I_1\left(\bar{k}a\right) + \gamma\nu_2\mathcal{F}_2(\nu_2 a)I_1'(\bar{k}a)\right]}{(\nu_2^2\gamma^2-k^2)\left[K_1\left(\bar{k}(a+t)\right) - \frac{K_1\left(\bar{k}d\right)I_1\left(\bar{k}(a+t)\right)}{I_1\left(\bar{k}d\right)}\right]},
\end{aligned} \tag{85}
$$

$$
\begin{aligned}
S_{12} = {} & \frac{\nu_2\left[\frac{\gamma\nu_2 a\mathcal{F}_1(\nu_2 a)I_1'(\bar{k}a)}{k\mu'} - a\mathcal{F}_3(\nu_2 a)I_1\left(\bar{k}a\right) - (a+t)\mathcal{F}_2(\nu_2 a)I_1(\bar{k}a)\right]}{\left[K_1\left(\bar{k}(a+t)\right) - \frac{K_1'\left(\bar{k}d\right)I_1\left(\bar{k}(a+t)\right)}{I_1'\left(\bar{k}d\right)}\right]} \\
& + \frac{j\gamma\beta\nu_2^2(a+t)\left[K_1'\left(\bar{k}(a+t)\right) - \frac{K_1\left(\bar{k}d\right)I_1'\left(\bar{k}(a+t)\right)}{I_1\left(\bar{k}d\right)}\right]I_1(\bar{k}a)\mathcal{F}_1(\nu_2 a)}{(\sigma_{2c}+j\omega\epsilon_0\epsilon')Z_0\left[K_1\left(\bar{k}(a+t)\right) - \frac{K_1'\left(\bar{k}d\right)I_1\left(\bar{k}(a+t)\right)}{I_1'\left(\bar{k}d\right)}\right]\left[K_1\left(\bar{k}(a+t)\right) - \frac{K_1\left(\bar{k}d\right)I_1\left(\bar{k}(a+t)\right)}{I_1\left(\bar{k}d\right)}\right]},
\end{aligned} \tag{86}
$$

$$
\begin{aligned}
S_{21} = {} & \frac{\nu_2\left[-\frac{aj\nu_2\beta\gamma\mathcal{F}_1(\nu_2 a)I_1'(\bar{k}a)}{Z_0(\sigma_{2c}+j\omega\epsilon_0\epsilon')} + a\mathcal{F}_3(\nu_2 a)I_1\left(\bar{k}a\right) + (a+t)I_1(\bar{k}a)\mathcal{F}_2(\nu_2 a)\right]}{\left[K_1\left(\bar{k}(a+t)\right) - \frac{K_1\left(\bar{k}d\right)I_1\left(\bar{k}(a+t)\right)}{I_1\left(\bar{k}d\right)}\right]} \\
& - \frac{\nu_2^2(a+t)\gamma\left[K_1'\left(\bar{k}(a+t)\right) - \frac{K_1'\left(\bar{k}d\right)I_1'\left(\bar{k}(a+t)\right)}{I_1'\left(\bar{k}d\right)}\right]I_1(\bar{k}a)\mathcal{F}_1(\nu_2 a)}{k\mu'\left[K_1\left(\bar{k}(a+t)\right) - \frac{K_1\left(\bar{k}d\right)I_1\left(\bar{k}(a+t)\right)}{I_1\left(\bar{k}d\right)}\right]\left[K_1\left(\bar{k}(a+t)\right) - \frac{K_1'\left(\bar{k}d\right)I_1\left(\bar{k}(a+t)\right)}{I_1'\left(\bar{k}d\right)}\right]},
\end{aligned} \tag{87}
$$

$$b_1 = \frac{\beta c a \nu_2^3 (a+t) I_1(\bar{k}r_{\rm b}) \left[\frac{jK_1(\bar{k}a)\mathcal{F}_3(\nu_2 a)}{\gamma} + \frac{\nu_2\beta K_1'(\bar{k}a)\mathcal{F}_1(\nu_2 a)}{(\sigma_{2c}+j\omega\epsilon_0\epsilon')Z_0}\right]\left[K_1'\left(\bar{k}(a+t)\right) - \frac{K_1(\bar{k}d)I_1'(\bar{k}(a+t))}{I_1(\bar{k}d)}\right]}{\pi r_{\rm b}\left(\frac{\nu_2^2\gamma^2}{k^2}-1\right)\left[K_1\left(\bar{k}(a+t)\right) - \frac{K_1'(\bar{k}d)I_1(\bar{k}(a+t))}{I_1'(\bar{k}d)}\right]\left[K_1\left(\bar{k}(a+t)\right) - \frac{K_1(\bar{k}d)I_1(\bar{k}(a+t))}{I_1(\bar{k}d)}\right]}$$
$$- \frac{\frac{jk\left(\frac{\nu_2^2\gamma^2}{k^2}-1\right)cI_1(\bar{k}r_{\rm b})K_1(\bar{k}a)\mathcal{F}_1(\nu_2 a)}{\beta\mu'\gamma}}{\pi r_{\rm b}\gamma\left[K_1\left(\bar{k}(a+t)\right) - \frac{K_1'(\bar{k}d)I_1(\bar{k}(a+t))}{I_1'(\bar{k}d)}\right]}$$
$$+ \frac{\frac{\nu_2^2 a(a+t)cI_1(\bar{k}r_{\rm b})[j\nu_2\beta\gamma K_1'(\bar{k}a)\mathcal{F}_2(\nu_2 a) - Z_0(\sigma_{2c}+j\omega\epsilon_0\epsilon')K_1(\bar{k}a)\mathcal{F}_4(\nu_2 a)]}{\gamma\left(\frac{\nu_2^2\gamma^2}{k^2}-1\right)}}{\pi r_{\rm b}\gamma\left[K_1\left(\bar{k}(a+t)\right) - \frac{K_1'(\bar{k}d)I_1(\bar{k}(a+t))}{I_1'(\bar{k}d)}\right]}, \tag{88}$$

$$b_2 = -\frac{jkcZ_0\nu_2(a+t)\mathcal{F}_2(\nu_2 a)I_1(\bar{k}r_{\rm b})K_1(\bar{k}a)}{\gamma^2\pi r_{\rm b}\left[K_1\left(\bar{k}(a+t)\right) - \frac{K_1(\bar{k}d)I_1(\bar{k}(a+t))}{I_1(\bar{k}d)}\right]} + \frac{c\nu_2(a+t)I_1(\bar{k}r_{\rm b})}{\gamma\pi r_{\rm b}\left[K_1\left(\bar{k}(a+t)\right) - \frac{K_1(\bar{k}d)I_1(\bar{k}(a+t))}{I_1(\bar{k}d)}\right]}$$
$$\times\left\{\frac{jZ_0\nu_2\mathcal{F}_1(\nu_2 a)K_1(\bar{k}a)\left[K_1'\left(\bar{k}(a+t)\right) - \frac{K_1'(\bar{k}d)I_1'(\bar{k}(a+t))}{I_1'(\bar{k}d)}\right]}{\mu'\left[K_1\left(\bar{k}(a+t)\right) - \frac{K_1'(\bar{k}d)I_1(\bar{k}(a+t))}{I_1'(\bar{k}d)}\right]}\right.$$
$$\left. - \frac{ja\bar{k}Z_0\mathcal{F}_3(\nu_2 a)K_1(\bar{k}a) + \frac{\nu_2 ak\beta\mathcal{F}_1(\nu_2 a)K_1'(\bar{k}a)}{(\sigma_{2c}+j\omega\epsilon_0\epsilon')}}{(a+t)}\right\}, \tag{89}$$

with

$$\mathcal{F}_1(z) = K_1(z)I_1\left(z\left(1+\frac{t}{a}\right)\right) - I_1(z)K_1\left(z\left(1+\frac{t}{a}\right)\right), \tag{90}$$

$$\mathcal{F}_2(z) = I_1'\left(z\left(1+\frac{t}{a}\right)\right)K_1(z) - I_1(z)K_1'\left(z\left(1+\frac{t}{a}\right)\right), \tag{91}$$

$$\mathcal{F}_3(z) = K_1'(z)I_1\left(z\left(1+\frac{t}{a}\right)\right) - I_1'(z)K_1\left(z\left(1+\frac{t}{a}\right)\right), \tag{92}$$

$$\mathcal{F}_4(z) = I_1'\left(z\left(1+\frac{t}{a}\right)\right)K_1'(z) - I_1'(z)K_1'\left(z\left(1+\frac{t}{a}\right)\right). \tag{93}$$

In the case of a thin extreme chamber $t = 0$, or a transparent chamber wall with $\sigma_{2c} = 0$, $\mu^{'} = 1$, and $\epsilon^{'} = 1$, direct calculations show that Eq. (82) reproduces the transverse non-relativistic space charge impedance per unit length $Z_{\rm non,\,sp,\,T}[d]$ for the perfectly conductive chamber with radius d after those parameters are plugged into Eq. (82), whereas the transverse non-relativistic space charge impedance $Z_{\rm non,\,sp,\,T}[a]$ with radius a is reproduced as σ_{2c} approaches infinity in Eq. (82).

After the indirect space charge impedance per unit length,

$$Z_{\rm non,spind,T}[a] = -\frac{kZ_0}{j2\pi r_{\rm b}\beta\gamma^3}I_1(\bar{k}r_{\rm b})\frac{K_1(\bar{k}a)}{I_1(\bar{k}a)}, \tag{94}$$

is introduced into Eq. (82), the transverse impedance $Z_T/\mathcal{L}$ can be divided into the resistive-wall part $Z_{\mathrm{T,\,RW}}$,

$$Z_{\mathrm{T,RW}} = -\frac{A(k)}{2c\beta\gamma} + \frac{kZ_0}{j2\pi r_b\beta\gamma^3} I_1(\bar{k}r_b)\frac{K_1(\bar{k}a)}{I_1(\bar{k}a)}, \tag{95}$$

and the space charge impedance $Z_{\mathrm{non,\,sp,\,T}}[a]$ with boundary condition per unit length.

The betatron tune is affected by the transverse impedance, which includes space charge effects. The contribution to the tune, like the longitudinal impedance, can be treated independently from a simulation standpoint [28,30], because the impedance can be divided into the space charge impedance with the perfectly conductive boundary and the resistive-wall impedance [21,26,30,31]. The particle-in-cell scheme (see, for example, Ref. [27]) is effective for evaluating the influence of the space charge effects with the boundary condition on the tune, while the contribution to the betatron tune shift by the resistive-wall impedance may be simulated by implementing the impedance source along the accelerators [28]. Analytically, the contribution from the space charge impedance with a perfectly conductive boundary can be evaluated using the classical Laslett theory [32], whereas the contribution from the resistive-wall impedance can be evaluated using the theory dealing with beam instabilities [2].

As d approaches infinity in Eq. (82) while keeping t constant, the formula for the transverse impedance of the resistive chamber with finite thickness is expressed as

$$\frac{Z_T}{\mathcal{L}} = -\frac{P_1}{Q_1} + \frac{kZ_0K_1[\bar{k}r_b]}{j2\pi r_b\beta\gamma^3}, \tag{96}$$

where

$$\begin{aligned}
P_1 = {} & kZ_0I_1[\bar{k}r_b]\big\{jk\beta\nu_2^2\big(k^2-\gamma^2\nu_2^2\big)^2 \\
& \times\big[jk(a+t)\beta\gamma\mu'\nu_2I_1[a\bar{k}]K_1'[\bar{k}(a+t)]\mathcal{F}_1(a\nu_2) \\
& - k(a+t)Z_0\mu'(\sigma_{2c}+j\epsilon_0\epsilon'\omega)I_1[a\bar{k}]K_1[\bar{k}(a+t)]\mathcal{F}_2(a\nu_2) \\
& + aZ_0(\sigma_{2c}+j\epsilon_0\epsilon'\omega)K_1[\bar{k}(a+t)](\gamma\nu_2I'[a\bar{k}]\mathcal{F}_1(a\nu_2) - k\mu'I_1[a\bar{k}]\mathcal{F}_3(a\nu_2))\big] \\
& \times\big[k(a+t)Z_0\mu'(\sigma_{2c}+j\epsilon_0\epsilon'\omega)K_1[a\bar{k}]K_1[\bar{k}(a+t)]\mathcal{F}_2(a\nu_2) \\
& - \gamma((a+t)Z_0\nu_2(\sigma_{2c}+j\epsilon_0\epsilon'\omega)K_1[a\bar{k}]K_1'[\bar{k}(a+t)]\mathcal{F}_1(a\nu_2) \\
& + j\mu'K_1[\bar{k}(a+t)](ak\beta\nu_2K_1'[a\bar{k}]\mathcal{F}_1[a\nu_2] + ja\bar{k}Z_0(\sigma_{2c}+j\epsilon_0\epsilon'\omega)K_1[a\bar{k}]\mathcal{F}_3[a\nu_2]))\big] \\
& + \big[(jZ_0(k^2-\gamma^2\nu_2^2)^2(\sigma_{2c}+j\epsilon_0\epsilon'\omega)K_1[a\bar{k}]K_1[\bar{k}(a+t)] \\
& - ak^3(a+t)\beta^3\gamma^2\mu'\nu_2^4K_1'[a\bar{k}]K_1'[\bar{k}(a+t)])\mathcal{F}_1(a\nu_2) \\
& + ak^3(a+t)Z_0\beta^2\gamma\mu'\nu_2^3(-j\sigma_{2c}+\epsilon_0\epsilon'\omega)K_1[\bar{k}(a+t)]K_1'[a\bar{k}]\mathcal{F}_2(a\nu_2) \\
& + ak^3(a+t)Z_0\beta^2\gamma\mu'\nu_2^3(-j\sigma_{2c}+\epsilon_0\epsilon'\omega)K_1[a\bar{k}]K_1'[\bar{k}(a+t)]\mathcal{F}_3(a\nu_2) \\
& + ak^3(a+t)Z_0^2\beta\mu'\nu_2^2(\sigma_{2c}+j\epsilon_0\epsilon'\omega)^2K_1[a\bar{k}]K_1[\bar{k}(a+t)]\mathcal{F}_4(a\nu_2)\big] \\
& \times\big[j\mu'(k^2-\gamma^2\nu_2^2)^2I_1[a\bar{k}]K_1[\bar{k}(a+t)]\mathcal{F}_1(a\nu_2) \\
& + ak(a+t)Z_0\beta\gamma^2\nu_2^3(\sigma_{2c}+j\epsilon_0\epsilon'\omega)K_1'[\bar{k}(a+t)](\nu_2I_1'[a\bar{k}]\mathcal{F}_1(a\nu_2) - \bar{k}\mu'I_1[a\bar{k}]\mathcal{F}_3(a\nu_2)) \\
& + ak^2(a+t)Z_0\beta\gamma\mu'\nu_2^2(\sigma_{2c}+j\epsilon_0\epsilon'\omega)K_1[\bar{k}(a+t)](-\nu_2I_1'[a\bar{k}]\mathcal{F}_2(a\nu_2) \\
& + \bar{k}\mu'I_1[a\bar{k}]\mathcal{F}_4(a\nu_2))\big]\big\},
\end{aligned} \tag{97}$$

$$
\begin{aligned}
Q_1 = 2\pi r_{\mathrm{b}}\beta\gamma^3\big\{&k\beta\nu_2^2(k^2-\gamma^2\nu_2^2)^2\\
&\times\big[jk(a+t)\beta\gamma\mu'\nu_2 I_1[a\bar{k}]K_1'[\bar{k}(a+t)]\mathcal{F}_1(a\nu_2)\\
&-k(a+t)Z_0\mu'(\sigma_{2c}+j\epsilon_0\epsilon'\omega)I_1[a\bar{k}]K_1[\bar{k}(a+t)]\mathcal{F}_2(a\nu_2)\\
&+aZ_0(\sigma_{2c}+j\epsilon_0\epsilon'\omega)K_1[\bar{k}(a+t)](\gamma\nu_2 I_1'[a\bar{k}]\mathcal{F}_1(a\nu_2)-k\mu' I_1[a\bar{k}]\mathcal{F}_3(a\nu_2))\big]\\
&\times\big[(a+t)Z_0\gamma\nu_2(\sigma_{2c}+j\epsilon_0\epsilon'\omega)I_1[a\bar{k}]K_1'[\bar{k}(a+t)]\mathcal{F}_1(a\nu_2)\\
&-k(a+t)Z_0\mu'(\sigma_{2c}+j\epsilon_0\epsilon'\omega)I_1[a\bar{k}]K_1[\bar{k}(a+t)]\mathcal{F}_2(a\nu_2)\\
&+k\mu' K_1[\bar{k}(a+t)](ja\beta\gamma\nu_2 I_1'[a\bar{k}]\mathcal{F}_1(a\nu_2)-aZ_0(\sigma_{2c}+j\epsilon_0\epsilon'\omega)I_1[a\bar{k}]\mathcal{F}_3(a\nu_2))\big]\\
&-\big[j\mu'(k^2-\gamma^2\nu_2^2)^2 I_1[a\bar{k}]K_1[\bar{k}(a+t)]\mathcal{F}_1(a\nu_2)\\
&+ak(a+t)Z_0\beta\gamma^2\nu_2^3(\sigma_{2c}+j\epsilon_0\epsilon'\omega)K_1'[\bar{k}(a+t)](\nu_2 I_1'[a\bar{k}]\mathcal{F}_1(a\nu_2)-\bar{k}\mu' I_1[a\bar{k}]\mathcal{F}_3(a\nu_2))\\
&+ak^2(a+t)Z_0\beta\gamma\mu'\nu_2^2(\sigma_{2c}+j\epsilon_0\epsilon'\omega)K_1[\bar{k}(a+t)](-\nu_2 I_1'[a\bar{k}]\mathcal{F}_2(a\nu_2)+\bar{k}\mu' I_1[a\bar{k}]\mathcal{F}_4(a\nu_2))\big]\\
&\times\big[Z_0\big(k^2-\gamma^2\nu_2^2\big)^2(\sigma_{2c}+j\epsilon_0\epsilon'\omega)I_1[a\bar{k}]K_1[\bar{k}(a+t)]\mathcal{F}_1(a\nu_2)\\
&+ak^3(a+t)\beta^2\gamma\mu'\nu_2^3 K_1'[\bar{k}(a+t)](j\beta\gamma\nu_2 I_1'[a\bar{k}]\mathcal{F}_1(a\nu_2)-Z_0(\sigma_{2c}+j\epsilon_0\epsilon'\omega)I_1[a\bar{k}]\mathcal{F}_3(a\nu_2))\\
&-ak^3(a+t)Z_0\beta\mu'\nu_2^2(\sigma_{2c}+j\epsilon_0\epsilon'\omega)K_1[\bar{k}(a+t)]\\
&\times(\beta\gamma\nu_2 I_1'[a\bar{k}]\mathcal{F}_2(a\nu_2)+jZ_0(\sigma_{2c}+j\epsilon_0\epsilon'\omega)I_1[a\bar{k}]\mathcal{F}_4(a\nu_2))\big]\big\}.
\end{aligned}
\tag{98}
$$

Figure 11 illustrates the Lorentz-γ dependence of Eq. (96). The red solid, blue solid, and black dashed lines represent the results with $\gamma = 10$, $\gamma = 1.2$ obtained using Eq. (96) after subtracting the non-relativistic space charge impedance $Z_{\mathrm{non,\,sp,\,T}}[a]$, i.e. Eq. (81), and the traditional resistive-wall impedance results with infinite thickness for an ultra-relativistic beam ($\beta = 1$) [2,17]:

$$
\frac{Z_{\mathrm{T}}}{\mathcal{L}} = \frac{2c}{\omega a^2}\frac{(1+j)}{2\pi a\sigma_{2c}}\sqrt{\frac{\omega\mu' Z_0\sigma_{2c}}{2c}}. \tag{99}
$$

Because the slow beam receives more kicks from the fluctuating RF fields while passing through the sine-like transverse wake fields [2,23], the transverse impedance for non-relativistic

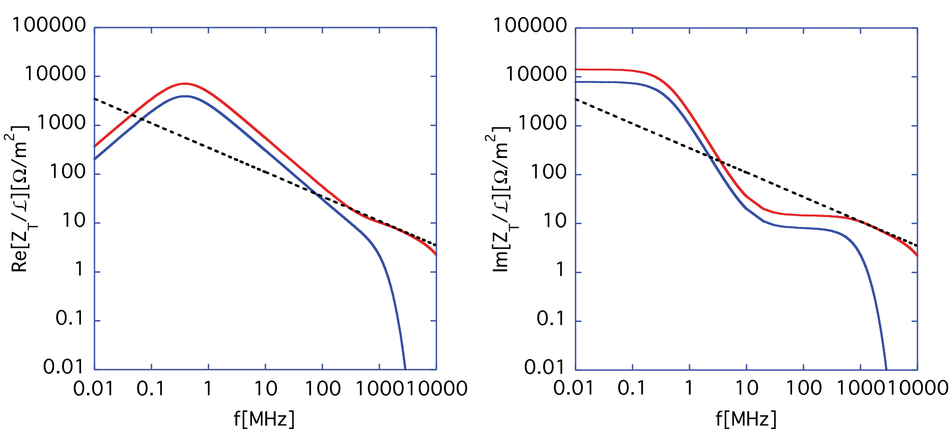

Fig. 11. Lorentz-γ dependence of transverse impedance excluding the space charge impedance for a chamber with a radius of $a = 65\,\mathrm{mm}$ and thickness $t = 0.1\,\mathrm{mm}$, where $r_{\mathrm{b}} = 1\,\mathrm{mm}$, $\sigma_{2c} = 10^5\,\mathrm{S\,m^{-1}}$, and $\epsilon' = \mu' = 1$. The red solid, blue solid, and black dashed lines represent the results using Eq. (96) with $\gamma = 10$, $\gamma = 1.2$, and the conventional resistive-wall impedance results of Eq. (99).

beams (blue) tends to be lower than that for relativistic beams (red). In Sects. 4.2 and 4.3 we demonstrate that the transverse impedance of the relativistic beams is roughly proportional to the Lorentz β.

As shown in the left panel of Fig. 11, the real part of the impedance for relativistic beams, such as $\gamma = 10$ (red), deviates from the traditional formula (black dashed) for the impedance in the frequency region where the skin depth δ is greater than the thickness of the chamber t (250 MHz in this example). Despite the fact that the real part of the impedance increases as the frequency decreases, the impedance reaches zero at the origin of the frequency ($f = 0$) after the peak is formed, due to the property of the transverse impedance [2].

4.2 *The case of an infinitely thick resistive chamber*

Equation (96) can be further simplified as the chamber thickness t approaches infinity, and the total transverse impedance for a thick resistive chamber with infinite t is expressed as

$$\begin{aligned}\frac{Z_{\rm T}}{\mathcal{L}} = &\left\{\frac{\nu_2\beta\gamma^2 kZ_0 a\nu_2^2 I_1(\bar{k}r_{\rm b})K_1(\nu_2 a)\left[-\bar{k}K_1'(\nu_2 a)I_1\left(\bar{k}a\right)+\frac{\nu_2 K_1(\nu_2 a)I_1'(\bar{k}a)}{\mu'}\right]}{2\gamma\pi r_{\rm b}(\nu_2^2\gamma^2-k^2)^2(\sigma_{2c}+j\omega\epsilon_0\epsilon')I_1\left(\bar{k}a\right)}\right\}\\
&\times\left\{\frac{Z_0\beta\gamma^2 k\nu_2^2 a^2\left[-\bar{k}K_1'(\nu_2 a)I_1\left(\bar{k}a\right)+\frac{\nu_2 K_1(\nu_2 a)I_1'(\bar{k}a)}{\mu'}\right]\left[\frac{j\nu_2\beta\gamma I_1'(\bar{k}a)K_1(\nu_2 a)}{(\sigma_{2c}+j\omega\epsilon_0\epsilon')Z_0}-I_1\left(\bar{k}a\right)K_1'(\nu_2 a)\right]}{\left(\nu_2^2\gamma^2-k^2\right)^2}\right.\\
&\left.-\frac{j\gamma K_1^2(\nu_2 a)I_1^2(\bar{k}a)}{k\mu'(\sigma_{2c}+j\omega\epsilon_0\epsilon')}\right\}^{-1}\\
&+Z_{\rm non,sp,T}[a],\end{aligned}\tag{100}$$

which is identical to the formula obtained following the procedure in Appendix A3 by assuming infinite d and t at the inception.

Equation (100) is approximated for a highly conductive chamber as

$$\begin{aligned}\frac{Z_{\rm T}}{\mathcal{L}} \simeq -&\left\{\frac{\nu_2\beta\gamma^2 kZ_0 a\nu_2^2 I_1(\bar{k}r_{\rm b})}{2\gamma\pi r_{\rm b}(\nu_2^2\gamma^2-k^2)^2(\sigma_{2c}+j\omega\epsilon_0\epsilon')I_1\left(\bar{k}a\right)}\left[\bar{k}I_1\left(\bar{k}a\right)+\frac{\nu_2 I_1'(\bar{k}a)}{\mu'}\right]\right\}\\
&\times\left\{-\frac{Z_0\beta\gamma^2 k\nu_2^2 a^2\left[\bar{k}I_1\left(\bar{k}a\right)+\frac{\nu_2 I_1'(\bar{k}a)}{\mu'}\right]\left[\frac{j\nu_2\beta\gamma I_1'(\bar{k}a)}{(\sigma_{2c}+j\omega\epsilon_0\epsilon')Z_0}+I_1\left(\bar{k}a\right)\right]}{(\nu_2^2\gamma^2-k^2)^2}+\frac{j\gamma I_1^2(\bar{k}a)}{k\mu'(\sigma_{2c}+j\omega\epsilon_0\epsilon')}\right\}^{-1}\\
&+Z_{\rm non,sp,T}[a],\end{aligned}\tag{101}$$

for non-relativistic beams, applying Eq. (41) for Eq. (100), and

$$\frac{Z_{\rm T}}{\mathcal{L}} \simeq \frac{\beta\frac{\mu'}{\pi a^2}\left(Z_0\sigma_{2c}+\frac{j\omega(-1+\beta^2\epsilon'\mu')}{c\beta^2\mu'}\right)}{\left[-j\mu'\sigma_{2c}+\left(-j\sigma_{2c}+\frac{\omega\epsilon'}{cZ_0}\right)a\sqrt{\frac{\omega^2(1-\beta^2\epsilon'\mu')}{c^2\beta^2}+\frac{j\omega\mu' Z_0\sigma_{2c}}{c}}\right]}+Z_{\rm non,sp,T}[a],\tag{102}$$

for relativistic beams, after approximating Eq. (101) for larger Lorentz γ, where

$$Z_{\rm rel,T,sp}[a] = \frac{Z_0}{j2\pi\beta\gamma^2}\left(\frac{1}{r_{\rm b}^2}-\frac{1}{a^2}\right).\tag{103}$$

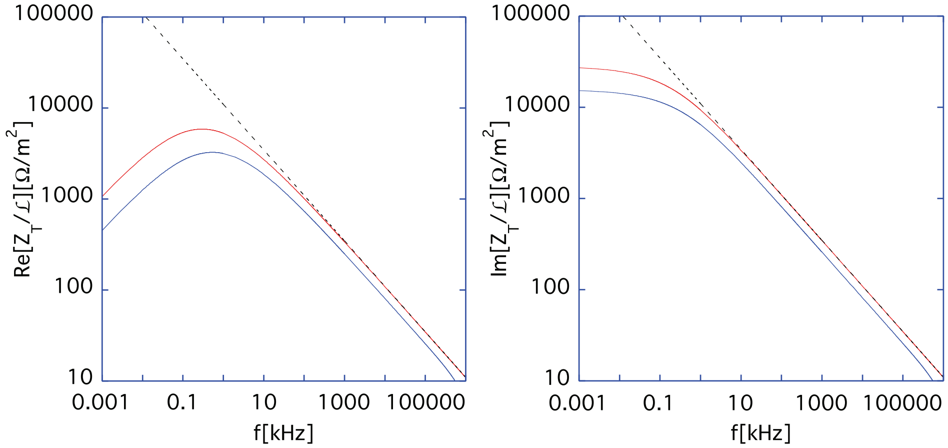

Fig. 12. Lorentz-γ dependence of the transverse impedance Z_T excluding the space charge impedance $Z_{\mathrm{non,\,sp,\,T}}[a]$ for a thick chamber with radius $a = 65\,\mathrm{mm}$, where $r_b = 1\,\mathrm{mm}$, $\sigma_{2c} = 10^5\,\mathrm{S\,m^{-1}}$, and $\epsilon' = \mu' = 1$. The red solid, blue solid, and black dashed lines represent the results of Eq. (101) with $\gamma = 10$, $\gamma = 1.2$, and the traditional resistive-wall impedance results from Eq. (99).

In this case, $Z_{\mathrm{rel,\,T,\,sp}}[a]$ is defined as the relativistic space charge impedance per unit length for a chamber with radius a [29]. Note that the Lorentz β is clearly expressed in $Z_{\mathrm{rel,\,T,\,sp}}[a]$ (compare Ref. [2, Eq. (2.79)]).

When we focus in particular on the frequency range in

$$\frac{c\mu'}{a^2 Z_0\sigma_{2c}} \lesssim \omega \ll \min\left[\frac{cZ_0\sigma_{2c}}{\epsilon'}, \frac{c\beta^2\mu' Z_0\sigma_{2c}}{|\beta^2\epsilon'\mu' - 1|}\right], \tag{104}$$

Eq. (102) becomes

$$\frac{Z_T}{\mathcal{L}} \simeq c\beta\sqrt{\frac{\mu'\omega Z_0\sigma_{2c}}{2c}}\frac{(1+j)}{\pi a^3\sigma_{2c}\omega} + Z_{\mathrm{rel,T,sp}}[a], \tag{105}$$

reproducing the conventional formula in Eq. (99) after $\beta = 1$ is plugged into Eq. (105). Hence, we find that the resistive-wall impedance (the first term) with infinite thickness is roughly proportional to the Lorentz β for relativistic beams.

Figure 12 illustrates the Lorentz-γ dependence of the transverse impedance, with the exception of the space charge impedance, for an infinitely thick chamber with radius $a = 65\,\mathrm{mm}$, where $r_b = 1\,\mathrm{mm}$, $\sigma_{2c} = 10^5\,\mathrm{S\,m^{-1}}$, and $\epsilon' = \mu' = 1$. The red solid, blue solid, and black dashed lines represent the results of Eq. (101) with $\gamma = 10$, $\gamma = 1.2$, and the conventional resistive-wall impedance results with Eq. (99). In this case, the frequency at the peak of the real part of the impedance is evaluated as

$$f \simeq \frac{c\mu'}{2\pi a^2 Z_0\sigma_{2c}} = 0.3\,\mathrm{kHz}, \tag{106}$$

as found by the lower limit of the inequality in Eq. (104), which is consistent with the left panel of Fig. 12, regardless of the Lorentz γ.

4.3 *The case of a finite-thickness chamber*

For a chamber satisfying $|\nu_2 a| \gg 1$ while keeping the thickness t and the outer chamber's radius d finite, the transverse impedance for relativistic beams is approximated as

$$\frac{Z_T}{\mathcal{L}} \simeq Z_{\mathrm{res}} + Z_{\mathrm{sp}} + Z_{\mathrm{sp},d} - j\frac{Z_0}{2\pi r_b^2\beta\gamma^2}, \tag{107}$$

where the final term represents the relativistic transverse direct space charge impedance, $Z_{\rm res}$ is defined as the resistive-wall contribution to the impedance, $Z_{\rm sp}$ and $Z_{{\rm sp},\,d}$ are the indirect space charge contributions due to the chamber with radius a and the outer chamber with radius d, respectively. They are clearly stated as

$$
\begin{aligned}
Z_{\rm res} = \beta\frac{2c}{\omega a^2}&\frac{1}{\left(\frac{1}{R_{\rm in}}+\frac{1}{j\omega L_{\rm in}}+j\omega C_{\rm in}\right)}\\
&-\left\{\frac{jZ_0}{2\pi\beta\gamma^2}\left[\frac{a[\nu_2+jka(\sigma_{2c}+j\omega\epsilon_0\epsilon')\beta Z_0\tanh\nu_2 t]\tanh\nu_2 t}{d^2\mu'\left(\frac{1}{(a+t)}+\frac{(a+t)}{d^2}\right)^2}\right.\right.\\
&\left.\left.+\frac{\nu_2\left(1+\frac{a^2}{d^2}\right)\tanh\nu_2 t}{(a+t)\mu'\left(\frac{1}{(a+t)^2}-\frac{(a+t)^2}{d^4}\right)}+\frac{4k^2\beta^2\left(\frac{1}{d^2}-\frac{1}{(a+t)^2}-\frac{a^2}{d^2(a+t)^2}\right)}{\left(\frac{1}{(a+t)^2}-\frac{(a+t)^2}{d^4}\right)^2}\right]\right\}\\
&\times\left\{\frac{a[\nu_2+jka(\sigma_{2c}+j\omega\epsilon_0\epsilon')\beta Z_0\tanh\nu_2 t]\tanh\nu_2 t}{\mu'\left(\frac{1}{(a+t)}+\frac{(a+t)}{d^2}\right)^2}+\frac{\nu_2 a^2\tanh\nu_2 t}{(a+t)\mu'\left(\frac{1}{(a+t)^2}-\frac{(a+t)^2}{d^4}\right)}\right.\\
&\left.-\frac{4k^2\beta^2a^2}{\left(\frac{1}{(a+t)^2}-\frac{(a+t)^2}{d^4}\right)^2(a+t)^2}\right\}^{-1},
\end{aligned}
\tag{108}
$$

$$Z_{\rm sp} = j\frac{Z_0}{2\pi a^2\beta\gamma^2}, \tag{109}$$

$$Z_{{\rm sp},d} = j\frac{Z_0}{2\pi d^2\beta\gamma^2}, \tag{110}$$

$$R_{\rm in} = \frac{\nu_2}{2\pi a(\sigma_{2c}+j\omega\epsilon_0\epsilon')\tanh\nu_2 t}, \tag{111}$$

$$L_{\rm in} = \frac{Z_0}{c}\frac{\left(1-\frac{(a+t)^2}{d^2}\right)}{2\pi\left(\frac{(2a+t)}{(a+t)}-\frac{t(a+t)}{d^2}\right)}, \tag{112}$$

$$C_{\rm in} = \frac{\epsilon_0 8\pi\mu' a}{\nu_2\left(1-\frac{(a+t)^2}{d^2}\right)^2\tanh\nu_2 t}, \tag{113}$$

after applying Eq. (41) and very large Lorentz γ to Eq. (82), i.e. the original formula for the total transverse impedance. As the second term of Eq. (108), proportional to γ^{-2}, compensates $Z_{{\rm sp},\,d}$ in Eq. (107) for a highly conductive "thick" inner chamber, Eq. (107) gives the resistive-wall impedance with the relativistic space charge impedance $Z_{\rm rel,\,sp,\,T}[a]$ for this case. Meanwhile, it compensates $Z_{\rm sp}$ in Eq. (107), and the first term of Eq. (108) vanishes for a thin extreme inner chamber, making Eq. (107) identical to the relativistic space charge impedance $Z_{\rm rel,\,sp,\,T}[d]$ with radius d.

We can successfully define the resistive-wall term $Z_{\rm res}$ as in Eq. (108), defining the inductance $L_{\rm in}$, the frequency-dependent dynamic resistance $R_{\rm in}$, and the capacitance $C_{\rm in}$ per meter produced by the chamber as in Eqs. (111), (112), and (113). Hence, we find that the resistive-wall impedance with finite thickness is roughly proportional to the Lorentz β for relativistic beams.

Using the Panofsky–Wenzel theorem [33], we discover that $R_{\rm in}$ in Eq. (108) can generate DC resistance for this resistive chamber even in the relativistic transverse impedance.

For most highly conductive thick chambers with finite t, Eq. (107) can be simplified as

$$\frac{Z_{\rm T}}{\mathcal{L}} \simeq \beta \frac{2c}{\omega a^2} \frac{1}{\left(\frac{1}{R_{\rm in}} + \frac{1}{j\omega L_{\rm in}}\right)} + Z_{\rm rel,sp,T}[a], \tag{114}$$

by neglecting the capacitive component. The conditions are expressed as

$$\frac{4k^2}{\left(\frac{1}{(a+t)} - \frac{(a+t)}{d^2}\right)\left(1 - \frac{(a+t)^4}{d^4}\right)\tanh\frac{t}{\delta}} \ll \frac{\frac{1}{\delta} + ka\sigma_{2c}Z_0\tanh\frac{t}{\delta}}{\mu'\left(\frac{a}{(a+t)} + \frac{a(a+t)}{d^2}\right)} + \frac{1}{\delta\mu'\left(1 - \frac{(a+t)^2}{d^2}\right)}, \tag{115}$$

$$\frac{1}{\delta\left(1 - \frac{(a+t)^2}{d^2}\right)} \ll \frac{\frac{1}{\delta} + ka\sigma_{2c}Z_0\tanh\frac{t}{\delta}}{\left(\frac{a}{(a+t)} + \frac{a(a+t)}{d^2}\right)}, \tag{116}$$

$$\frac{1}{\delta} \ll ka\sigma_{2c}Z_0\tanh\frac{t}{\delta}, \tag{117}$$

$$\omega \ll \frac{\sigma_{2c}}{\epsilon_0\epsilon'}. \tag{118}$$

When we focus on the frequency range denoted by

$$1 \ll |\nu_2 t|, \qquad \frac{c\mu'}{a^2\beta^2\sigma_{2c}Z_0}\left[1 + \frac{a\left(\frac{1}{(a+t)} + \frac{(a+t)}{d^2}\right)}{(a+t)\left(\frac{1}{(a+t)} - \frac{(a+t)}{d^2}\right)}\right]^2 \ll \omega < \frac{\sigma_{2c}}{\epsilon_0\epsilon'}, \tag{119}$$

for ultra-relativistic beams ($\beta = 1$), the first term of Eq. (114) reproduces the conventional resistive-wall impedance (Eq. (99)).

At low frequency, especially when

$$\frac{1}{a\sigma_{2c}Z_0 t} + \frac{\left(\frac{1}{(a+t)} + \frac{(a+t)}{d^2}\right)}{\sigma_{2c}Z_0 t(a+t)\left(\frac{1}{(a+t)} - \frac{(a+t)}{d^2}\right)} \lesssim \frac{\omega}{c} < \frac{2}{t^2 Z_0\mu'\sigma_{2c}}, \tag{120}$$

the impedance with Eq. (114) differs from the standard formula (Eq. (99)), resulting in

$$\frac{Z_{\rm T}}{\mathcal{L}} \simeq \beta \frac{2c}{\omega a^2} \frac{1}{\left[\sigma_{2c}2\pi at + \frac{1}{j\omega L_{\rm in}}\right]} + Z_{\rm rel,sp,T}[a]. \tag{121}$$

The first term in the denominator of Eq. (121) represents the admittance of the DC resistance. The upper bound of the inequality in Eq. (120) comes from $\delta > t$. Although the skin depth δ is greater than the thickness of the chamber t in the frequency region, the DC dipole wall-current continues to flow in the chamber wall, and the real part of the impedance is increased when compared to the conventional transverse impedance (Eq. (99)).

At the low frequency extreme given by

$$0 \le \frac{\omega}{c} \lesssim \frac{1}{a\sigma_{2c}Z_0 t} + \frac{\left(\frac{1}{(a+t)} + \frac{(a+t)}{d^2}\right)}{\sigma_{2c}Z_0 t(a+t)\left(\frac{1}{(a+t)} - \frac{(a+t)}{d^2}\right)}, \tag{122}$$

the formula is approximated as

$$\frac{Z_{\rm T}}{\mathcal{L}} \simeq \beta \frac{2c}{\omega a^2}\left(2\pi\sigma_{2c}\omega^2 at L_{\rm in}^2 + j\omega L_{\rm in}\right) + Z_{\rm rel,sp,T}[a]. \tag{123}$$

Consequently, the real part of the impedance approaches zero toward the origin of frequency, while the imaginary part approaches a constant, which is consistent with the property of the transverse impedance as stated in Sect. 4.1 [2].

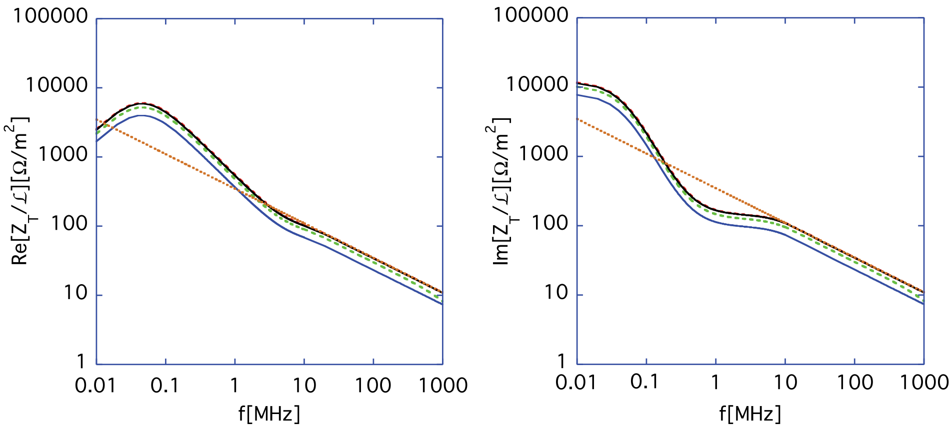

Fig. 13. Comparison of the transverse impedance calculated by Eq. (82), minus the space charge impedance of Eq. (81), and that calculated by Eq. (107) minus Eq. (103), where $t = 1$ mm, $a = 65$ mm, $d = 165$ mm, $r_b = 1$ mm, $\sigma_{2c} = 10^5\,\mathrm{S\,m^{-1}}$, and $\epsilon' = \mu' = 1$. The brown doted lines denote the traditional resistive-wall impedance results obtained by Eq. (99). The solid lines denote the approximate results of Eq. (107) without Eq. (103), while the dashed lines are the rigorous results of Eq. (82) without Eq. (81). The red and black lines represent the outcome for $\gamma = 10$, while the green and blue lines represent the outcome for $\gamma = 2$.

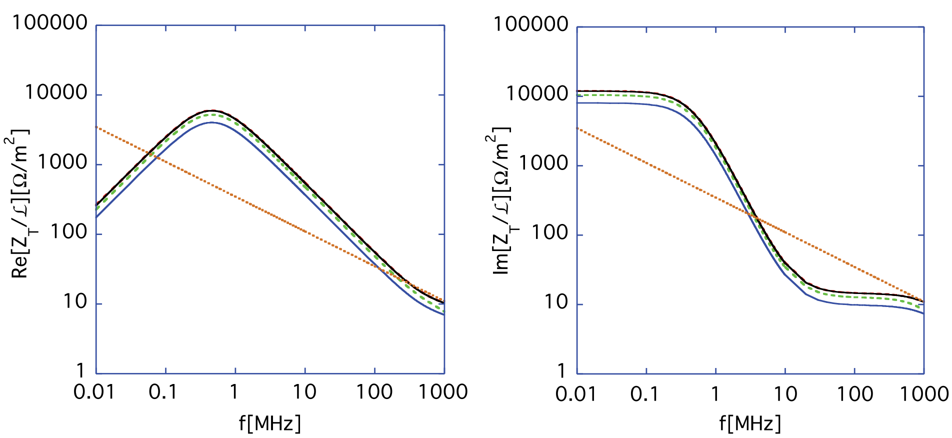

Fig. 14. Comparison of the transverse impedance calculated by Eq. (82), minus the space charge impedance of Eq. (81), and that calculated by Eq. (107) minus Eq. (103), where $t = 0.1$ mm, $a = 65$ mm, $d = 165$ mm, $r_b = 1$ mm, $\sigma_{2c} = 10^5\,\mathrm{S\,m^{-1}}$, and $\epsilon' = \mu' = 1$. The brown dotted lines denote the traditional resistive-wall impedance results obtained by Eq. (99). The solid lines denote the approximate results of Eq. (107) without Eq. (103), while the dashed lines represent the rigorous results obtained by Eq. (82) without Eq. (81). The red and black lines represent the outcome for $\gamma = 10$, while the green and blue lines represent the outcome for $\gamma = 2$.

Figures 13 and 14 show a comparison of the rigorous transverse impedance calculated by Eq. (82), minus the non-relativistic space charge impedance calculated by Eq. (81), and the approximate relativistic transverse impedance from Eq. (107) minus the relativistic space charge impedance calculated by Eq. (103), where $a = 65$ mm, $d = 165$ mm, $r_b = 1$ mm, $\sigma_{2c} = 10^5\,\mathrm{S\,m^{-1}}$, and $\epsilon' = \mu' = 1$. The results for $t = 1$ mm and $t = 0.1$ mm are shown in Figs. 13 and 14, respectively.

The brown dotted lines in both figures represent the conventional resistive-wall impedance results from Eq. (99). The solid lines provide the approximate results of Eq. (107) in the absence of Eq. (103), while the dashed lines denote the rigorous results of Eq. (82) in the absence of

Eq. (81). The red and black lines represent the result for $\gamma = 10$, while the green and blue lines represent the result for $\gamma = 2$.

Figures 13 and 14 demonstrate that Eq. (107) accurately reproduces the impedance for relativistic beams ($\gamma = 10$) because the red and black lines are almost identical, while the green and blue lines ($\gamma = 2$) differ, indicating a limit of the large Lorentz-γ approximation. All the results deviate from the conventional resistive-wall impedance (brown) at the frequency where the skin depth δ is greater than the thickness of the chamber t, which is given by $f \lesssim 2.5\,\mathrm{MHz}$ and $f \lesssim 250\,\mathrm{MHz}$ in Figs. 13 and 14, respectively. According to the lower limit of the condition in Eq. (120), the frequency at which the real part of the impedance reaches its maximum is evaluated by

$$f = \frac{c}{2\pi a\sigma_{2c}Z_0 t} + \frac{c\left(\frac{1}{(a+t)} + \frac{(a+t)}{d^2}\right)}{2\pi\sigma_{2c}Z_0 t(a+t)\left(\frac{1}{(a+t)} - \frac{(a+t)}{d^2}\right)} \simeq 0.039\,\mathrm{MHz}\ \text{for}\ t = 1\,\mathrm{mm},$$

$$\simeq 0.39\,\mathrm{MHz}\ \text{for}\ t = 0.1\,\mathrm{mm}, \tag{124}$$

which adequately explains the results of both Figs. 13 and 14. Figures 13 and 14 demonstrate that the resistive chamber at the low frequency extreme produces the pure inductance L_{in} given by Eq. (112), which is the origin of the imaginary part of the impedance.

The question here is why the dipole wall-current can continue to flow in the resistive chamber wall in the frequency range specified by Eq. (120) where the skin depth δ is greater than the thickness of the resistive chamber t, though the monopole current begins to flow on the perfectly conductive chamber at $\rho = d$ in the frequency range.

Equation (121) suggests that the pure inductance L_{in} produced by the chamber in conjunction with the frequency-dependent dynamic resistance R_{in} plays a significant role in causing the phenomenon. Moreover, by introducing the dynamic capacitance C_{in}, we can deal with the resistive-wall impedance as well as the space charge impedance at the same time, because it is infinite for an infinitesimal chamber (see Eq. (113)).

In particular, the transverse impedance of relativistic beams at low frequencies is approximated as

$$\frac{Z_{\mathrm{T}}}{\mathcal{L}} \simeq \left\{\left[\frac{1}{\frac{\omega a^2}{2c\beta}\left(\frac{1}{j\omega L_{\mathrm{in}}} + \frac{1}{R_{\mathrm{in}}}\right)} + j\frac{Z_0\left(\frac{1}{a^2} - \frac{1}{d^2}\right)}{2\pi\beta\gamma^2}\right]^{-1} + j\frac{\omega^2 a^2 C_{\mathrm{in}}}{2c\beta}\right\}^{-1} + j\frac{Z_0\left(\frac{1}{d^2} - \frac{1}{r_{\mathrm{b}}^2}\right)}{2\pi\beta\gamma^2}, \tag{125}$$

based on the model of a parallel electric circuit. The inductance, resistance, and capacitance due to the chamber are represented by the first and third terms in the first term of Eq. (125). The second term there refers to the difference in indirect space charge impedances due to the inner and outer chambers. The final term represents the relativistic space charge impedance for a chamber with radius d. For infinitesimal t, the impedance produces the space charge impedance $Z_{\mathrm{rel,\,sp,\,T}}[d]$ in Eq. (125) because the dynamic capacitance C_{in} becomes infinite.

The corresponding description based on the parallel circuit model is given by Eq. (69) for the longitudinal impedance. Comparing these expressions leads to the conclusion that the monopole and dipole currents perceive the surrounding environment, which consists of the resistive chamber, vacuum layer, and perfectly conductive chamber, as having different impedances.

Figure 15 compares the transverse impedance calculated by Eq. (107) and that calculated by Eq. (125), where $\gamma = 10$, $t = 1\,\mathrm{mm}$, $a = 65\,\mathrm{mm}$, $d = 1065\,\mathrm{mm}$, $r_{\mathrm{b}} = 1\,\mathrm{mm}$, $\sigma_{2c} = 10^5\,\mathrm{S\,m^{-1}}$,

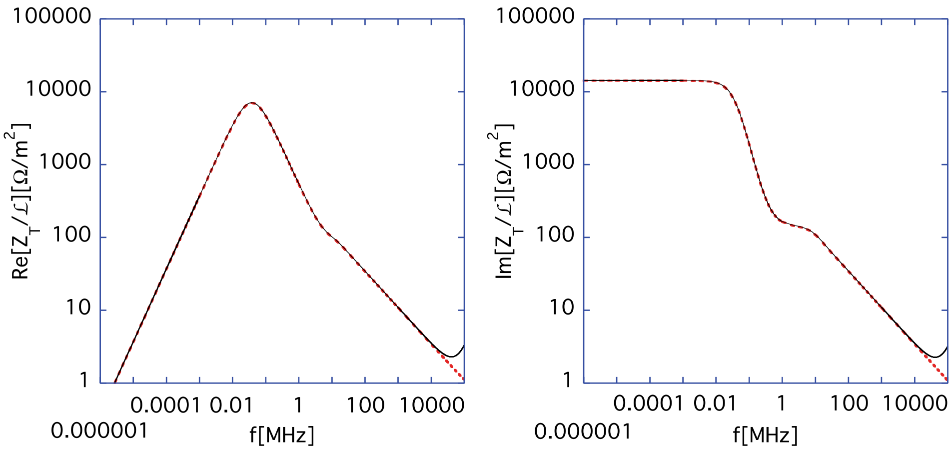

Fig. 15. Comparison of the transverse impedance calculated by Eq. (107) and that calculated by Eq. (125), where $\gamma = 10$, $t = 1$ mm, $a = 65$ mm, $d = 1065$ mm, $r_b = 1$ mm, $\sigma_{2c} = 10^5\,\mathrm{S\,m^{-1}}$, and $\epsilon' = \mu' = 1$. The space charge impedance given by Eq. (103) is subtracted in both cases. The red dashed lines denote the results of Eq. (107) in the absence of Eq. (103), and the solid black lines are the results of Eq. (125) in the absence of Eq. (103).

and $\epsilon' = \mu' = 1$. The relativistic space charge impedance given by Eq. (103) is subtracted in both results. The red dashed lines represent the results of Eq. (107) without $Z_{\mathrm{rel,\,sp,\,T}}[a]$ from Eq. (103), and the solid black lines represent the results of Eq. (125) without $Z_{\mathrm{rel,\,sp,\,T}}[a]$ as calculated by Eq. (103). This example shows that, up to 1 GHz, Eq. (125) with the parallel circuit model accurately approximates the relativistic transverse impedance calculated by Eq. (107).

Here, we hypothetically disregard the inductance L_{in} in Eq. (125), resulting in

$$\frac{Z_{\mathrm{T}}}{\mathcal{L}} \simeq \left\{ \left[\frac{1}{\frac{\omega a^2}{2c\beta}\left(\frac{2\pi\sigma_{2c}a\delta\tanh(1+j)\frac{t}{\delta}}{(1+j)}\right)} + j\frac{Z_0\left(\frac{1}{a^2}-\frac{1}{d^2}\right)}{2\pi\beta\gamma^2} \right]^{-1} + j\frac{\omega^2 a^2 C_{\mathrm{in}}}{2c\beta} \right\}^{-1} + j\frac{Z_0\left(\frac{1}{d^2}-\frac{1}{r_b^2}\right)}{2\pi\beta\gamma^2}. \tag{126}$$

Figure 16 compares the real part of the rigorous transverse impedance calculated by Eq. (107) (red dashed) to the hypothetical impedance calculated by Eq. (126) (black solid). The results show that the energy loss of the beam would be greater at low frequencies if the dipole wall-current continued to flow in the resistive chamber wall rather than converting to the displacement current.

Because R_{in}, L_{in}, and C_{in} do not effectively depend on the Lorentz γ, and have significant values for any value of d, the transverse impedance can create the frequency region where the DC resistance appears. In this sense, the dipole current always perceives the resistive chamber as the LRC circuit impedance, regardless of whether the beams are relativistic or not.

As a result, description of the transverse impedance based on the parallel circuit model helps us understand that the transverse impedance is determined to minimize the energy loss of the beam. The dipole wall-current continues to flow in the resistive chamber wall in the frequency region where the skin depth is greater than the thickness of the chamber until the energy loss of the beam can be minimized by converting the wall-current to the displacement current flowing outside the wall proper.

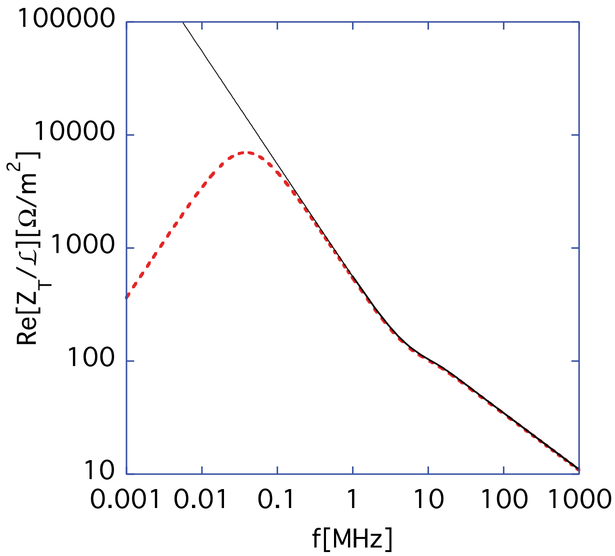

Fig. 16. Comparison of the transverse impedance calculated by Eq. (107) (red dashed) and that calculated by Eq. (126) (solid black), where $\gamma = 10$, $t = 1$ mm, $a = 65$ mm, $d = 1065$ mm, $r_b = 1$ mm, $\sigma_{2c} = 10^5$ S m^{-1}, and $\epsilon^{'} = \mu^{'} = 1$. The space charge impedance given by Eq. (103) is subtracted in both cases.

When we focus on the case of far extreme d, the transverse impedance for a highly conductive chamber is simplified as

$$\frac{Z_\mathrm{T}}{\mathcal{L}} \simeq \left\{\frac{Z_0\left\{\left[4k^2a(a+t)\beta^2 - \frac{k^2t^2}{\gamma^2}\right]\mu' + 2\gamma^2\beta^2\nu_2(a+t)\tanh(\nu_2 t) + (1+\beta^2)\gamma^2\mu'\tanh^2(\nu_2 t)\right\}}{j2a^2\pi\beta\gamma^2}\right\}$$
$$\times\left\{\left[4k^2a(a+t)\beta^2 - \frac{k^2t^2}{\gamma^2}\right]\mu' - (2a+t)\nu_2\tanh(\nu_2 t) - jak(a+t)Z_0\beta\sigma_{2c}\tanh^2(\nu_2 t)\right\}^{-1}$$
$$+\left[\frac{Z_0}{j2\pi r_\mathrm{b}^2\beta\gamma^2} - \frac{Z_0}{j2\pi a^2\beta\gamma^2}\right], \tag{127}$$

at low frequency by using Eq. (82), regardless of whether the beam is relativistic or not, where the final term represents the space charge impedance $Z_{\mathrm{rel,\,sp,\,T}}[a]$. Note that Eq. (127) produces

$$\frac{Z_\mathrm{T}}{\mathcal{L}} \simeq \beta\cdot c\sqrt{\frac{\mu'\omega Z_0\sigma_{2c}}{2c}}\frac{(1+j)}{\pi a^3\sigma_{2c}\omega} + Z_{\mathrm{rel,sp,T}}[a], \tag{128}$$

by increasing σ_{2c}, while it produces the space charge impedance $Z_{\mathrm{rel,\,sp,\,T}}[d]$ for infinitesimal t. When focusing on the high frequency region where the skin depth is much less than the chamber thickness t, it is preferable to use Eq. (100) to evaluate the transverse impedance.

Figure 17 illustrates a comparison of the rigorous results of Eq. (96) (solid) with the exception of the space charge impedance $Z_{\mathrm{non,\,sp,\,T}}[a]$ and the approximate results from Eq. (127) (dashed) minus $Z_{\mathrm{rel,\,sp,\,T}}[a]$. The parameters are as follows: $a = 65$ mm, $t = 1$ mm, $r_\mathrm{b} = 1$ mm, $\sigma_{2c} = 10^5$ S m^{-1}, and $\epsilon^{'} = \mu^{'} = 1$. The results with $\gamma = 10$ and $\gamma = 1.2$ are represented by the red solid, blue dashed, and black solid, green dashed lines, respectively. The purple dotted lines represent the traditional resistive-wall impedance results obtained by Eq. (99). The approximate results, regardless of whether the beam is relativistic or not, explain well the rigorous ones below 100 MHz in this example.

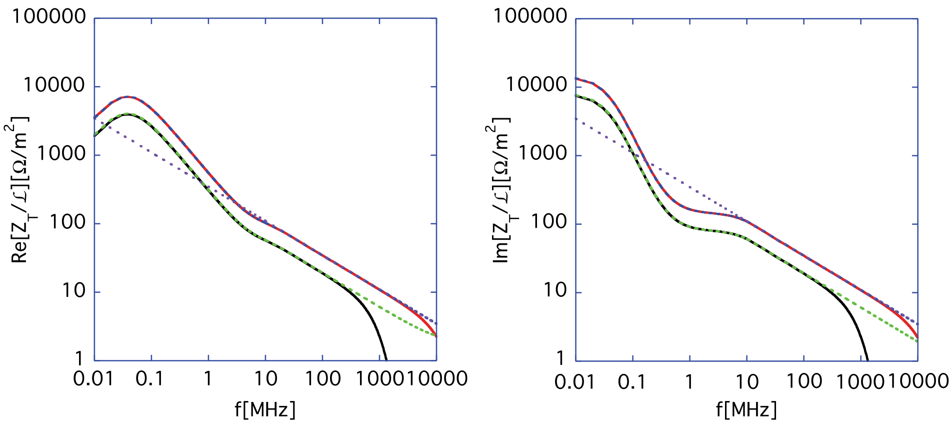

Fig. 17. Comparison of Eq. (96) (solid) with the exception of the space charge impedance $Z_{\mathrm{non,\,sp,\,T}}[a]$ and Eq. (127) (dashed) minus $Z_{\mathrm{rel,\,sp,\,T}}[a]$, where $a = 65\,\mathrm{mm}$, $t = 1\,\mathrm{mm}$, $r_{\mathrm{b}} = 1\,\mathrm{mm}$, $\sigma_{2c} = 10^5\,\mathrm{S\,m^{-1}}$, and $\epsilon^{'} = \mu^{'} = 1$. The results with $\gamma = 10$ and $\gamma = 1.2$ are represented by the red solid, blue dashed and black solid, green dashed lines, respectively. The purple dotted lines denote the traditional resistive-wall impedance results obtained by Eq. (99).

5. Conclusions

In this report we have presented a comprehensive picture of the two-dimensional resistive-wall impedance with a finite thickness in combination with the space charge impedance obtained by introducing a perfectly conductive chamber through a vacuum layer outside the original resistive chamber. We can simulate the conventional situation in which only the resistive chamber exists in space by increasing the distance between the outer surface of the resistive chamber and the inner surface of the perfectly conductive chamber. The method corrects the longitudinal resistive-wall impedance described in Ref. [1] for relativistic beams, compromising the picture based on the parallel circuit model and the description in Ref. [2].

Equation (75) approximates well the longitudinal impedance at low frequency, whereas Eq. (127) does so for the transverse impedance at low frequency, regardless of whether the beam is relativistic or not. However, if we focus on the high frequency region where the skin depth is less than the chamber thickness t we should use Eqs. (34) and (100) for the longitudinal and transverse impedances, respectively.

Even if the skin depth is more than the chamber thickness, the longitudinal resistive-wall impedance with finite thickness does not produce DC resistance for relativistic beams. On the other hand, the longitudinal impedance for a non-relativistic beam, as well as the transverse impedance, can create a DC resistance dominant region when the skin depth is greater than the chamber thickness. The electric parallel circuit model can be used to understand the characteristics.

When the skin depth is greater than the chamber thickness, the monopole wall current flows dominantly on the imaginary chamber wall at infinity (which corresponds to the introduced perfectly conductive chamber outside the resistive chamber), rather than continuing to flow on the inner thin real chamber wall, explaining the rapid decrease of the longitudinal resistive-wall impedance for relativistic beams while retaining the direct space charge force. Meanwhile, the space between the resistive and perfectly conductive chamber functions as a high impedance region for non-relativistic beams. Therefore, in the case of non-relativistic beams, the monopole wall current can continue to flow on the resistive chamber when the skin depth exceeds the chamber thickness.

The dipole current always perceives the resistive chamber as the LRC circuit impedance whose resistance produces DC resistance for the infinitesimal thick chamber. After all, regardless of whether the beam is relativistic or not, the transverse impedance produces a DC resistance dominant region when the skin depth exceeds the chamber thickness. However, because the impedance is chosen to minimize the energy loss of the beam, the real part of the impedance creates a peak at a very low frequency before descending to zero at the frequency origin, whereas the imaginary part of the impedance converges to be pure inductive with space charge impedance for the inner chamber. In other words, even when the skin depth is greater than the chamber thickness, the dipole wall-current continues to flow in the resistive chamber wall until the energy loss of the beam can be minimized by converting the wall-current to the displacement current flowing outside the wall proper.

This picture leads us to the conclusion that monopole and dipole currents perceive the surrounding environment, which consists of the resistive chamber, vacuum layer, and perfectly conductive chamber, as having different impedances.

Hence, not only the longitudinal but also the transverse resistive-wall impedances, including the space charge impedance, are determined to minimize the energy loss of the beam, even in the two-dimensional resistive-wall chamber with finite thickness, as in the case of a 2.5-dimensional short ceramic break with titanium nitride coating.

Acknowledgments

The author would like to express gratitude to all members of the J-PARC project at JAEA/KEK. The author would like to thank Dr. N. Hayashi for encouraging him to write this paper. This work was partially supported by JSPS KAKENHI Grant No. JP17K05124.

Appendix A. Derivation of the resistive-wall impedance

A.1 Particular solutions of the Maxwell equations with beam charge and current densities

Assume that a particle moves along a beam pipe with velocity βc in the longitudinal direction, where β is the Lorentz β and c is the velocity of light. The Maxwell equations can be written as wave equations. If we assume that electromagnetic fields have a time dependency of $e^{j\omega t}$, the Maxwell equations become the Helmholtz equations:

$$(\Delta + k^2\beta^2)\vec{E} = jk\beta Z_0\vec{j} + \vec{\nabla}(cZ_0\bar{\rho}), \tag{A1}$$

$$(\Delta + k^2\beta^2)\vec{H} = -\vec{\nabla} \times \vec{j}, \tag{A2}$$

where j is the imaginary unit; $\bar{\rho}$ and $\vec{j}$ are the charge and current densities of the beam, respectively; $k = \omega/\beta c$; and $Z_0 = 120\pi$ [Ω] is the impedance of free space. The wave equations for the longitudinal component of the electric and magnetic field contain no transverse field component in the cylindrical coordinates (ρ, θ, z) for an axially symmetric structure. They are no longer linked. There is a source term $cZ_0\partial\bar{\rho}/\partial z + jk\beta Z_0 j_z$ for the longitudinal field, whereas the z-component of $\vec{\nabla} \times \vec{j}$ vanishes for particles with only longitudinal velocity.

When a beam with charge q travels along the pipe at the constant radial offset position $\rho = r_{\rm b}$, $\theta = \theta_{\rm b}$, the charge density is expressed as

$$\bar{\rho} = \frac{i_m \delta(\rho - r_b)\delta_p(\theta - \theta_b)\delta(z - \beta ct)}{r_b^{1+m}} = \sum_{m=0}^{\infty} \int \frac{dk}{2\pi} i_m \rho_m, \tag{A3}$$

$$\rho_m = \frac{\delta(\rho - r_b)\cos m(\theta - \theta_b) e^{-jk(z-\beta ct)}}{\pi r_b^{1+m}(1 + \delta_{m,0})}, \tag{A4}$$

$$i_m = q r_b^m, \tag{A5}$$

where $\delta(x)$ is the δ-function; $\delta_p(\theta)$ is the periodic δ-function; and $\delta_{m,n}$ is the Kronecker δ. Because the general solution of the Maxwell equations is obtained by superposing those for $i_m\rho_m$, we select $i_m\rho_m$ as the source term. Let us define the source field specified with superscript S as the solution that satisfies the Maxwell equations with ρ_m, $\vec{j}_m = (0, 0, c\beta\rho_m)$ and vanishes at $\rho \to \infty$. It is provided by

$$H_\rho^S = E_\theta^S = H_z^S = 0; \tag{A6}$$

$$E_z^S = \begin{cases} \frac{jkcZ_0 I_0(\bar{k}r_b)}{2\pi\gamma^2} K_0(\bar{k}\rho) e^{-jkz} & \text{for } \rho > r_b, \\ \frac{jkcZ_0 K_0(\bar{k}r_b)}{2\pi\gamma^2} I_0(\bar{k}\rho) e^{-jkz} & \text{for } r_b > \rho; \end{cases} \tag{A7}$$

$$\frac{\beta}{Z_0} E_\rho^S = H_\theta^S = \begin{cases} \frac{\beta kc I_0(\bar{k}r_b)}{2\pi\gamma} K_1(\bar{k}\rho) e^{-jkz} & \text{for } \rho > r_b, \\ -\frac{\beta kc K_0(\bar{k}r_b)}{2\pi\gamma} I_1(\bar{k}\rho) e^{-jkz} & \text{for } r_b > \rho; \end{cases} \tag{A8}$$

for $m = 0$, and

$$H_z^S = 0; \tag{A9}$$

$$E_z^S = \begin{cases} \frac{jkcZ_0 I_m(\bar{k}r_b)}{\pi r_b^m \gamma^2} K_m(\bar{k}\rho) \cos m(\theta - \theta_b) e^{-jkz} & \text{for } \rho > r_b, \\ \frac{jkcZ_0 K_m(\bar{k}r_b)}{\pi r_b^m \gamma^2} I_m(\bar{k}\rho) \cos m(\theta - \theta_b) e^{-jkz} & \text{for } r_b > \rho; \end{cases} \tag{A10}$$

$$-\frac{Z_0}{\beta} H_\rho^S = E_\theta^S = \begin{cases} \frac{mcZ_0 I_m(\bar{k}r_b)}{\rho\pi r_b^m} K_m(\bar{k}\rho) \sin m(\theta - \theta_b) e^{-jkz} & \text{for } \rho > r_b, \\ \frac{mcZ_0 K_m(\bar{k}r_b)}{\rho\pi r_b^m} I_m(\bar{k}\rho) \sin m(\theta - \theta_b) e^{-jkz} & \text{for } r_b > \rho; \end{cases} \tag{A11}$$

$$\frac{\beta}{Z_0} E_\rho^S = H_\theta^S = \begin{cases} \frac{\beta kc I_m(\bar{k}r_b)}{2\pi r_b^m \gamma} (K_{m-1}(\bar{k}\rho) + K_{m+1}(\bar{k}\rho)) \cos m(\theta - \theta_b) e^{-jkz} & \text{for } \rho > r_b, \\ -\frac{\beta kc K_m(\bar{k}r_b)}{2\pi r_b^m \gamma} (I_{m-1}(\bar{k}\rho) + I_{m+1}(\bar{k}\rho)) \cos m(\theta - \theta_b) e^{-jkz} & \text{for } r_b > \rho; \end{cases} \tag{A12}$$

for $m > 0$, where γ is the Lorentz γ, $\bar{k} = k/\gamma$, and $K_m(z)$ and $I_m(z)$ are the modified Bessel functions [24].

When a cylindrical beam with the current density $j_z = \beta c(1 - \Theta(\rho - \sigma))e^{-jkz}/(\pi\sigma^2)$, where $\Theta(x)$ is the step function, passes through the chamber, the source fields ($E_z^{(S)}$ and $H_\theta^{(S)}$) for the beam are calculated as

$$\begin{aligned} E_z^{(S)} &= \frac{jkcZ_0 e^{-jkz}}{\pi\sigma^2\gamma^2} \left[\int_0^\rho dr_b r_b I_0(\bar{k}r_b) K_0(\bar{k}\rho) + \int_\rho^\sigma dr_b r_b K_0(\bar{k}r_b) I_0(\bar{k}\rho) \right] \\ &= \frac{jcZ_0}{\pi\gamma\sigma^2} \left(\frac{1}{\bar{k}} - \sigma I_0(\bar{k}\rho) K_1(\bar{k}\sigma) \right) e^{-jkz} \qquad \text{for } \rho \le \sigma, \end{aligned} \tag{A13}$$

$$E_z^{(S)} = \frac{jkcZ_0 e^{-jkz}}{\pi\sigma^2\gamma^2} \int_0^\sigma dr_b r_b I_0(\bar{k}r_b) K_0(\bar{k}\rho) = \frac{jcZ_0}{\pi\sigma\gamma} I_1(\bar{k}\sigma) K_0(\bar{k}\rho) e^{-jkz} \quad \text{for } \rho \ge \sigma, \tag{A14}$$

$$H_\theta^{(\mathrm{S})} = \int_0^\rho dr_\mathrm{b} r_\mathrm{b} \frac{\beta kc I_0(\bar{k} r_\mathrm{b})}{\pi\gamma\sigma^2} K_1(\bar{k}\rho) e^{-jkz} - \int_\rho^\sigma dr_\mathrm{b} r_\mathrm{b} \frac{\beta kc K_0(\bar{k} r_\mathrm{b})}{\pi\gamma\sigma^2} I_1(\bar{k}\rho) e^{-jkz}$$

$$= \frac{\beta c I_1(\bar{k}\rho) K_1(\bar{k}\sigma)}{\pi\sigma} e^{-jkz} \qquad \text{for } \rho \leq \sigma, \tag{A15}$$

$$H_\theta^{(\mathrm{S})} = \int_0^\sigma dr_\mathrm{b} r_\mathrm{b} \frac{\beta kc I_0(\bar{k} r_\mathrm{b})}{\pi\gamma\sigma^2} K_1(\bar{k}\rho) e^{-jkz} = \frac{\beta c I_1(\bar{k}\sigma)}{\pi\sigma} K_1(\bar{k}\rho) e^{-jkz} \qquad \text{for } \rho \geq \sigma. \tag{A16}$$

A.2 Longitudinal impedance

Let us solve the Maxwell equations in this section such that the solution satisfies the boundary conditions due to the chamber walls ($\rho = a$, $\rho = a + t$, and $\rho = d$), and obtain the longitudinal resistive-wall impedance of the beam.

The general Maxwell equation solutions for $m = 0$ are expressed as

$$E_z = \frac{jcZ_0}{\pi\gamma\sigma^2} \left[\frac{1}{\bar{k}} - \sigma I_0(\bar{k}\rho) K_1(\bar{k}\sigma) \right] e^{-jkz} + \tilde{A}(k) e^{-jkz} I_0\left(\bar{k}\rho\right) \qquad \text{for } \rho \leq \sigma, \tag{A17}$$

$$E_z = \frac{jcZ_0 I_1(\bar{k}\sigma) K_0(\bar{k}\rho)}{\pi\sigma\gamma} e^{-jkz} + \tilde{A}(k) e^{-jkz} I_0\left(\bar{k}\rho\right) \qquad \text{for } \rho \geq \sigma, \tag{A18}$$

$$H_\theta = \frac{\beta c I_1(\bar{k}\rho) K_1(\bar{k}\sigma)}{\pi\sigma} e^{-jkz} + \frac{j\beta\gamma}{Z_0} \tilde{A}(k) e^{-jkz} I_1\left(\bar{k}\rho\right) \qquad \text{for } \rho \leq \sigma, \tag{A19}$$

$$H_\theta = \frac{\beta c I_1(\bar{k}\sigma) K_1(\bar{k}\rho)}{\pi\sigma} e^{-jkz} + \frac{j\beta\gamma}{Z_0} \tilde{A}(k) e^{-jkz} I_1\left(\bar{k}\rho\right) \qquad \text{for } \rho \geq \sigma, \tag{A20}$$

in the vacuum chamber ($\rho \leq a$),

$$E_z = e^{-jkz} (\tilde{C}_1(k) I_0(\nu_2\rho) + \tilde{C}_2(k) K_0(\nu_2\rho)), \tag{A21}$$

$$H_\theta = \frac{(\sigma_{2c} + j\omega\epsilon'\epsilon_0) e^{-jkz} (\tilde{C}_1(k) I_1(\nu_2\rho) - \tilde{C}_2(k) K_1(\nu_2\rho))}{\nu_2}, \tag{A22}$$

in the conductive material with conductivity σ_{2c}, relative dielectric constant $\epsilon^{'}$, and relative permeability $\mu^{'}$ ($a < \rho \leq a + t$), and

$$E_z = \tilde{D}_1(k) e^{-jkz} I_0\left(\bar{k}\rho\right) + \tilde{D}_2(k) e^{-jkz} K_0\left(\bar{k}\rho\right), \tag{A23}$$

$$H_\theta = \frac{j\beta\gamma}{Z_0} \tilde{D}_1(k) e^{-jkz} I_1\left(\bar{k}\rho\right) - \frac{j\beta\gamma}{Z_0} \tilde{D}_2(k) e^{-jkz} K_1\left(\bar{k}\rho\right), \tag{A24}$$

in the vacuum chamber ($a + t < \rho \leq d$), where $\nu_2 = \sqrt{k^2(1 - \beta^2\epsilon'\mu') + jk\beta\mu' Z_0\sigma_{2c}}$, and $\tilde{A}(k)$, $\tilde{C}_1(k)$, $\tilde{C}_2(k)$, $\tilde{D}_1(k)$, and $\tilde{D}_2(k)$ are arbitrary coefficients.

The matching conditions [1, Chap. 9] on each surface are specified by $\rho = a$, $\rho = a + t$, and $\rho = d$:

$$\frac{jcZ_0 I_1(\bar{k}\sigma) K_0(\bar{k}a)}{\pi\sigma\gamma} + \tilde{A}(k) I_0\left(\bar{k}a\right) = \tilde{C}_1(k) I_0(\nu_2 a) + \tilde{C}_2(k) K_0(\nu_2 a), \tag{A25}$$

$$\frac{\beta c I_1(\bar{k}\sigma) K_1(\bar{k}a)}{\pi\sigma} + \frac{j\beta\gamma}{Z_0} \tilde{A}(k) I_1\left(\bar{k}a\right)$$

$$= \frac{(\sigma_{2c} + j\omega\epsilon'\epsilon_0)}{\nu_2} (\tilde{C}_1(k) I_1(\nu_2 a) - \tilde{C}_2(k) K_1(\nu_2 a)), \tag{A26}$$

$$\tilde{C}_1(k)I_0\left(\nu_2(a+t)\right)+\tilde{C}_2(k)K_0\left(\nu_2(a+t)\right)$$
$$=\tilde{D}_1(k)I_0\left(\bar{k}(a+t)\right)+\tilde{D}_2(k)K_0\left(\bar{k}(a+t)\right), \tag{A27}$$

$$\frac{(\sigma_{2c}+j\omega\epsilon'\epsilon_0)}{\nu_2}\tilde{C}_1(k)I_1\left(\nu_2(a+t)\right)-\frac{(\sigma_{2c}+j\omega\epsilon'\epsilon_0)}{\nu_2}\tilde{C}_2(k)K_1\left(\nu_2(a+t)\right)$$
$$=\frac{j\beta\gamma}{Z_0}\tilde{D}_1(k)I_1\left(\bar{k}(a+t)\right)-\frac{j\beta\gamma}{Z_0}\tilde{D}_2(k)K_1\left(\bar{k}(a+t)\right), \tag{A28}$$

$$\tilde{D}_1(k)I_0\left(\bar{k}d\right)+\tilde{D}_2(k)K_0\left(\bar{k}d\right)=0. \tag{A29}$$

These equations comprise five linear equations with five unknown coefficients $\tilde{A}$, $\tilde{C}_1$, $\tilde{C}_2$, $\tilde{D}_1$, and $\tilde{D}_2$. Consequently, they give the unique solution of the coefficient $\tilde{A}(k)$ in a straightforward manner.

When the longitudinal impedance $Z_{\rm L}$ is defined as the average of the longitudinal electric field (normalized by the beam current) over the cross-section of the beam,

$$\frac{Z_{\rm L}}{\mathcal{L}}\equiv-\frac{2}{c\beta\sigma^2}\int_0^{\sigma}d\rho\rho E_z(\rho)e^{jkz}=-\frac{j2Z_0}{\bar{k}\beta\sigma^2\pi\gamma}\left[\frac{1}{2}-I_1(\bar{k}\sigma)K_1(\bar{k}\sigma)\right]-\frac{2\tilde{A}(k)I_1\left(\bar{k}\sigma\right)}{c\beta\sigma\bar{k}}, \tag{A30}$$

it is written as

$$\frac{Z_{\rm L}}{\mathcal{L}}=-\frac{j2Z_0}{\bar{k}\pi\beta\gamma\sigma^2}\left[\frac{1}{2}-I_1(\bar{k}\sigma)K_1(\bar{k}\sigma)\right]-\frac{2I_1\left(\bar{k}\sigma\right)}{\bar{k}\sigma c\beta}\frac{cI_1(\bar{k}\sigma)jZ_0\mathcal{N}(k)}{\pi\sigma\gamma\mathcal{D}(k)}, \tag{A31}$$

after the solved $\tilde{A}(k)$ is substituted into Eq. (A30), where $\mathcal{L}$ is the chamber length; $\mathcal{N}(k)$ and $\mathcal{D}(k)$ are calculated using Eqs. (23)–(28).

A.3 Transverse impedance

General solutions (in particular E_z, E_θ, H_z, and H_θ) for $m=1$ are expressed as

$$E_z=i_1(E_z^{\rm S}+A(k)I_1\left(\bar{k}\rho\right)\cos(\theta-\theta_{\rm b})e^{-jkz}), \tag{A32}$$

$$H_\theta=i_1\left(H_\theta^{\rm S}+\frac{j\gamma}{\bar{k}}\left(\frac{B(k)I_1(\bar{k}\rho)}{\rho}+\frac{\beta\bar{k}A(k)}{Z_0}I_1'(\bar{k}\rho)\right)\cos(\theta-\theta_{\rm b})e^{-jkz}\right), \tag{A33}$$

$$H_z=i_1B(k)I_1\left(\bar{k}\rho\right)\sin(\theta-\theta_{\rm b})e^{-jkz}, \tag{A34}$$

$$E_\theta=i_1\left(E_\theta^{\rm S}-\frac{j\beta\gamma Z_0}{\bar{k}}\left(\bar{k}B(k)I_1'(\bar{k}\rho)+\frac{A(k)}{Z_0\beta\rho}I_1(\bar{k}\rho)\right)\sin(\theta-\theta_{\rm b})e^{-jkz}\right), \tag{A35}$$

inside the vacuum chamber ($\rho<a$),

$$E_z=i_1(C_3(k)I_1\left(\nu_2\rho\right)+C_4(k)K_1\left(\nu_2\rho\right))\cos(\theta-\theta_{\rm b})e^{-jkz}, \tag{A36}$$

$$H_\theta=i_1\frac{jk}{\nu_2^2}\left[\frac{(C_1(k)I_1\left(\nu_2\rho\right)+C_2(k)K_1\left(\nu_2\rho\right))}{\rho}\right.$$
$$\left.+\frac{(\sigma_{2c}+j\omega\epsilon_0\epsilon')\nu_2(C_3(k)I_1'\left(\nu_2\rho\right)+C_4(k)K_1'\left(\nu_2\rho\right))}{jk}\right]\cos(\theta-\theta_{\rm b})e^{-jkz}, \tag{A37}$$

$$H_z=i_1(C_1(k)I_1\left(\nu_2\rho\right)+C_2(k)K_1\left(\nu_2\rho\right))\sin(\theta-\theta_{\rm b})e^{-jkz}, \tag{A38}$$

$$E_\theta = -i_1 \frac{jk}{\nu_2^2}\left[\frac{(C_3(k)I_1(\nu_2\rho) + C_4(k)K_1(\nu_2\rho))}{\rho}\right.$$
$$\left. + \beta Z_0 \mu' \nu_2 (C_1(k)I_1'(\nu_2\rho) + C_2(k)K_1'(\nu_2\rho))\right]\sin(\theta-\theta_\mathrm{b})e^{-jkz}, \qquad \text{(A39)}$$

in the conductive material ($a < \rho < a+t$), and

$$E_z = i_1\left[-E_4(k)\frac{K_1\left(\bar{k}d\right)}{I_1\left(\bar{k}d\right)}I_1\left(\bar{k}\rho\right) + E_4(k)K_1\left(\bar{k}\rho\right)\right]\cos(\theta-\theta_\mathrm{b})e^{-jkz}, \qquad \text{(A40)}$$

$$H_\theta = i_1\frac{j\gamma}{\bar{k}}\left[-E_2(k)\frac{K_1'\left(\bar{k}d\right)}{I_1'\left(\bar{k}d\right)}\frac{I_1\left(\bar{k}\rho\right)}{\rho} + E_2(k)\frac{K_1\left(\bar{k}\rho\right)}{\rho}\right.$$
$$\left. - E_4(k)\frac{K_1\left(\bar{k}d\right)}{I_1\left(\bar{k}d\right)}\frac{\beta\bar{k}I_1'\left(\bar{k}\rho\right)}{Z_0} + E_4(k)\frac{\beta\bar{k}K_1'\left(\bar{k}\rho\right)}{Z_0}\right]\cos(\theta-\theta_\mathrm{b})e^{-jkz}, \qquad \text{(A41)}$$

$$H_z = i_1\left[-E_2(k)\frac{K_1'\left(\bar{k}d\right)}{I_1'\left(\bar{k}d\right)}I_1\left(\bar{k}\rho\right) + E_2(k)K_1\left(\bar{k}\rho\right)\right]\sin(\theta-\theta_\mathrm{b})e^{-jkz}, \qquad \text{(A42)}$$

$$E_\theta = -i_1\frac{j\gamma}{\bar{k}}\left[\frac{E_4(k)}{\rho}\left(K_1\left(\bar{k}\rho\right) - \frac{K_1\left(\bar{k}d\right)I_1\left(\bar{k}\rho\right)}{I_1\left(\bar{k}d\right)}\right)\right.$$
$$\left. + \beta Z_0\bar{k}E_2(k)\left(K_1'\left(\bar{k}\rho\right) - \frac{K_1'\left(\bar{k}d\right)I_1'\left(\bar{k}\rho\right)}{I_1'\left(\bar{k}d\right)}\right)\right]\sin(\theta-\theta_\mathrm{b})e^{-jkz}, \qquad \text{(A43)}$$

outside the chamber ($a+t < \rho < d$), where $A(k)$, $B(k)$, $C_1(k)$, $C_2(k)$, $C_3(k)$, $C_4(k)$, $E_2(k)$, and $E_4(k)$ are arbitrary coefficients that are determined by the boundary conditions on $\rho = a$,

$$C_1(k)I_1(\nu_2 a) + C_2(k)K_1(\nu_2 a) = B(k)I_1\left(\bar{k}a\right), \qquad \text{(A44)}$$

$$C_1(k)I_1'(\nu_2 a) + C_2(k)K_1'(\nu_2 a) = \frac{jk\left(\frac{\nu_2^2\gamma^2}{k^2}-1\right)cZ_0 I_1(\bar{k}r_\mathrm{b})K_1(\bar{k}a)}{\beta Z_0\mu'\nu_2\gamma^2 a\pi r_\mathrm{b}}$$
$$+ \frac{\left(\frac{\nu_2^2\gamma^2}{k^2}-1\right)I_1(\bar{k}a)}{a\beta Z_0\mu'\nu_2}A(k) + \frac{\nu_2\gamma I_1'(\bar{k}a)}{k\mu'}B(k), \qquad \text{(A45)}$$

$$C_3(k)I_1(\nu_2 a) + C_4(k)K_1(\nu_2 a) = \frac{jkcZ_0 I_1(\bar{k}r_\mathrm{b})}{\pi r_\mathrm{b}\gamma^2}K_1(\bar{k}a) + A(k)I_1\left(\bar{k}a\right), \qquad \text{(A46)}$$

$$C_3(k)I_1'(\nu_2 a) + C_4(k)K_1'(\nu_2 a) = -\frac{k\nu_2\beta c I_1(\bar{k}r_\mathrm{b})K_1'(\bar{k}a)}{\pi r_\mathrm{b}\gamma(\sigma_{2c}+j\omega\epsilon_0\epsilon')} + \frac{j\nu_2\beta\gamma I_1'(\bar{k}a)}{Z_0(\sigma_{2c}+j\omega\epsilon_0\epsilon')}A(k)$$
$$+ \frac{jk\left(\frac{\nu_2^2\gamma^2}{k^2}-1\right)I_1(\bar{k}a)}{a(\sigma_{2c}+j\omega\epsilon_0\epsilon')\nu_2}B(k), \qquad \text{(A47)}$$

and on $\rho = a+t$,

$$C_1(k)I_1\left(\nu_2(a+t)\right)+C_2(k)K_1\left(\nu_2(a+t)\right)=E_2(k)\left[K_1\left(\bar{k}(a+t)\right)-\frac{K_1'\left(\bar{k}d\right)I_1\left(\bar{k}(a+t)\right)}{I_1'\left(\bar{k}d\right)}\right], \tag{A48}$$

$$\begin{aligned} &C_1(k)I_1'\left(\nu_2(a+t)\right)+C_2(k)K_1'\left(\nu_2(a+t)\right)\\ &=E_2(k)\frac{\nu_2\gamma\left[K_1'\left(\bar{k}(a+t)\right)-\frac{K_1'\left(\bar{k}d\right)I_1'\left(\bar{k}(a+t)\right)}{I_1'\left(\bar{k}d\right)}\right]}{k\mu'}\\ &\quad+E_4(k)\frac{\nu_2\gamma^2\left(1-\frac{k^2}{\nu_2^2\gamma^2}\right)\left[K_1\left(\bar{k}(a+t)\right)-\frac{K_1\left(\bar{k}d\right)I_1\left(\bar{k}(a+t)\right)}{I_1\left(\bar{k}d\right)}\right]}{k^2\beta Z_0\mu'(a+t)}, \end{aligned} \tag{A49}$$

$$C_3(k)I_1\left(\nu_2(a+t)\right)+C_4(k)K_1\left(\nu_2(a+t)\right)=E_4(k)\left[K_1\left(\bar{k}(a+t)\right)-\frac{K_1\left(\bar{k}d\right)I_1\left(\bar{k}(a+t)\right)}{I_1\left(\bar{k}d\right)}\right], \tag{A50}$$

$$\begin{aligned} &C_3(k)I_1'\left(\nu_2(a+t)\right)+C_4(k)K_1'\left(\nu_2(a+t)\right)\\ &=\frac{E_2(k)j\nu_2\gamma^2\left(1-\frac{k^2}{\nu_2^2\gamma^2}\right)\left[K_1\left(\bar{k}(a+t)\right)-\frac{K_1'\left(\bar{k}d\right)I_1\left(\bar{k}(a+t)\right)}{I_1'\left(\bar{k}d\right)}\right]}{k(\sigma_{2c}+j\omega\epsilon_0\epsilon')(a+t)}\\ &\quad+\frac{E_4(k)j\nu_2\gamma\beta\left[K_1'\left(\bar{k}(a+t)\right)-\frac{K_1\left(\bar{k}d\right)I_1'\left(\bar{k}(a+t)\right)}{I_1\left(\bar{k}d\right)}\right]}{(\sigma_{2c}+j\omega\epsilon_0\epsilon')Z_0}. \end{aligned} \tag{A51}$$

Note that Eqs. (A40)–(A43) already satisfy the boundary conditions $E_z(d)=E_\theta(d)=0$ on $\rho=d$.

Using the Panofsky–Wenzel theorem [2,33], we obtain the expression for the transverse impedance including a well-defined space charge impedance as

$$\frac{Z_\mathrm{T}}{\mathcal{L}}=-\frac{A(k)}{2c\beta\gamma}+\frac{kZ_0K_1(\bar{k}r_\mathrm{b})}{j2\pi r_\mathrm{b}\beta\gamma^3}, \tag{A52}$$

where r_b is finite.

Appendix B. Longitudinal impedances of the ceramic chambers with thin titanium nitride coating, covered by a perfectly conductive wall

In this section we derive Eq. (19) for the longitudinal impedances of ceramic chambers with translation symmetry, where the inner surface is coated with thin titanium nitride and the outer surface is surrounded by a perfectly conductive wall.

When a beam with current density $j_z=\beta c(1-\Theta(\rho-\sigma))e^{-jkz}/(\pi\sigma^2)$ passes through the chamber, E_z and H_θ in a vacuum are expressed as

$$E_z=\frac{jk}{\gamma^2}\frac{cZ_0}{\pi\sigma^2}\left(\frac{1}{\bar{k}^2}-\frac{\sigma I_0(\bar{k}\rho)K_1(\bar{k}\sigma)}{\bar{k}}\right)+\bar{A}_0(k)I_0(\bar{k}\rho), \tag{B1}$$

$$H_\theta = \frac{\beta c}{\pi\sigma} K_1(\bar{k}\sigma) I_1(\bar{k}\rho) + \frac{j\beta\gamma}{Z_0} \bar{\mathcal{A}}_0(k) I_1\left(\bar{k}\rho\right), \tag{B2}$$

for $\rho < \sigma$, and

$$E_z = \frac{jcZ_0}{\pi\sigma\gamma} I_1(\bar{k}\sigma) K_0(\bar{k}\rho) + \bar{\mathcal{A}}_0(k) I_0(\bar{k}\rho), \tag{B3}$$

$$H_\theta = \frac{\beta c}{\pi\sigma} I_1(\bar{k}\sigma) K_1(\bar{k}\rho) + \frac{j\beta\gamma}{Z_0} \bar{\mathcal{A}}_0(k) I_1\left(\bar{k}\rho\right), \tag{B4}$$

for $\sigma < \rho < a$, where $\bar{\mathcal{A}}_0(k)$ is an expansion coefficient, σ is the radius of the beam, and $\Theta(x)$ is the step function.

Inside the thin titanium nitride (for $a < \rho < a + t$) with high conductivity σ_{2c}, the fields are approximated as

$$E_z \simeq \bar{B}_0 I_0(\kappa_{\rm TiN}\rho) + \bar{C}_0 K_0(\kappa_{\rm TiN}\rho), \tag{B5}$$

$$H_\theta \simeq \frac{\kappa_{\rm TiN}}{jk\beta Z_0}(\bar{B}_0 I_1(\kappa_{\rm TiN}\rho) - \bar{C}_0 K_1(\kappa_{\rm TiN}\rho)), \tag{B6}$$

where $\kappa_{\rm TiN}$ is given by Eq. (5). In this case, $\bar{B}_0$ and $\bar{C}_0$ are the expansion coefficients.

Inside the ceramic (for $a + t < \rho < a_2$) with relative dielectric constant ϵ_1, they are expanded as

$$E_z = \bar{D}_0 I_0(\mu^k\rho) + \bar{E}_0 K_0(\mu^k\rho), \tag{B7}$$

$$H_\theta = -\frac{k\beta\epsilon_1}{j\mu^k Z_0}[\bar{D}_0 I_1(\mu^k\rho) - \bar{E}_0 K_1(\mu^k\rho)], \tag{B8}$$

using the expansion coefficients $\bar{D}_0$ and $\bar{E}_0$, where $\mu^k = \sqrt{k^2 - k^2\beta^2\epsilon_1}$.

When we assume the case of thin titanium nitride, the fields on $\rho = a$ and those on $\rho = a_2$ are referred to as

$$E_z(a_2) = A_0(a_2, a)E_z(a) + C_0(a_2, a)H_\theta(a), \tag{B9}$$

$$H_\theta(a_2) = I_0(a_2, a)E_z(a) + K_0(a_2, a)H_\theta(a), \tag{B10}$$

based on the field-matching techniques [1, Chap. 9], where the transfer coefficients $A_0(a_2, a)$, $C_0(a_2, a)$, $I_0(a_2, a)$, and $K_0(a_2, a)$ are approximated as

$$\begin{aligned} A_0(a_2, a) \simeq\ & \mu^k a(I_0'(\mu^k a)K_0(\mu^k a_2) - I_0(\mu^k a_2)K_0'(\mu^k a))\cosh\kappa_{\rm TiN}t \\ & - \frac{jZ_0(\mu^k)^2 a\sigma_{2c}(I_0(\mu^k a_2)K_0(\mu^k a) - I_0(\mu^k a)K_0(\mu^k a_2))\sinh\kappa_{\rm TiN}t}{k\beta\epsilon_1\kappa_{\rm TiN}}, \end{aligned} \tag{B11}$$

$$\begin{aligned} C_0(a_2, a) \simeq\ & \frac{\mu^k a(I_0'(\mu^k a)K_0(\mu^k a_2) - I_0(\mu^k a_2)K_0'(\mu^k a))\kappa_{\rm TiN}\sinh\kappa_{\rm TiN}t}{\sigma_{2c}} \\ & - \frac{jZ_0(\mu^k)^2 a(I_0(\mu^k a_2)K_0(\mu^k a) - I_0(\mu^k a)K_0(\mu^k a_2))\cosh\kappa_{\rm TiN}t}{k\beta\epsilon_1}, \end{aligned} \tag{B12}$$

$$\begin{aligned} I_0(a_2, a) \simeq\ & \frac{jk\beta a\epsilon_1(I_0'(\mu^k a)K_0'(\mu^k a_2) - I_0'(\mu^k a_2)K_0'(\mu^k a))\cosh\kappa_{\rm TiN}t}{Z_0} \\ & + \frac{\mu^k a\sigma_{2c}(I_0'(\mu^k a_2)K_0(\mu^k a) - I_0(\mu^k a)K_0'(\mu^k a_2))\sinh\kappa_{\rm TiN}t}{\kappa_{\rm TiN}}, \end{aligned} \tag{B13}$$

$$K_0(a_2, a) \simeq \frac{jk\beta a\epsilon_1 (I_0'(\mu^k a)K_0'(\mu^k a_2) - I_0'(\mu^k a_2)K_0'(\mu^k a))\kappa_{\text{TiN}} \sinh \kappa_{\text{TiN}} t}{\sigma_{2c} Z_0}$$
$$+ \mu^k a(I_0'(\mu^k a_2)K_0(\mu^k a) - I_0(\mu^k a)K_0'(\mu^k a_2)) \cosh \kappa_{\text{TiN}} t. \tag{B14}$$

The coefficient $\bar{\mathcal{A}}_0(k)$ in Eq. (B1) is obtained by solving Eq. (B9) after substituting Eqs. (B3), (B4), and the condition $E_z(a_2) = 0$ into Eq. (B9).

Equation (A30) provides the longitudinal impedance including space charge impedance, where $\tilde{\mathcal{A}}(k)$ is replaced by $\bar{\mathcal{A}}_0(k)$. To subtract the contribution due to space charge impedance from the final expression of the impedance of the ceramic chamber, the coefficient $\bar{\mathcal{A}}_0^{\text{perf}}(k)$, corresponding to the case that perfectly conductive walls exist on $\rho = a$, would be calculated in advance, and it is given by

$$\bar{\mathcal{A}}_0^{\text{perf}}(k) = -\frac{jcZ_0}{\pi\sigma\gamma I_0(\bar{k}a)} I_1(\bar{k}\sigma)K_0(\bar{k}a). \tag{B15}$$

Finally, the longitudinal impedance is expressed as

$$Z_{\text{L}} = Z_{\text{non,sp}}(a) + Z_{\text{L,ceramic}}, \tag{B16}$$

where

$$Z_{\text{non,sp}}(a) = -\frac{jZ_0}{\beta\pi k\sigma^2}\left(1 - 2I_1(\bar{k}\sigma)K_1(\bar{k}\sigma) - \frac{2I_1^2(\bar{k}\sigma)K_0(\bar{k}a)}{I_0(\bar{k}a)}\right)\mathcal{L}, \tag{B17}$$

$$Z_{\text{L,ceramic}} = \frac{2\mathcal{L}C_0(a_2, a)I_1^2(\bar{k}\sigma)}{\pi\sigma^2\bar{k}^2 a I_0^2(\bar{k}a)\left[A_0(a_2, a) + C_0(a_2, a)\frac{j\beta\gamma I_1(\bar{k}a)}{Z_0 I_0(\bar{k}a)}\right]}, \tag{B18}$$

$Z_{\text{non, sp}}(a)$ is the space charge impedance, $Z_{\text{L, ceramic}}$ is the impedance of a ceramic chamber covered by a perfectly conductive wall with a titanium nitride coating, and $\mathcal{L}$ is the length of the chamber.

In the case of $a_1 \simeq a_2$, after substituting Eqs. (B11) and (B12) into Eq. (B18), Eq. (B18) is expressed as

$$Z_{\text{L,ceramic}} = \frac{\mathcal{L}}{2\pi a}\left[\frac{\left[\frac{\kappa_{\text{TiN}}}{\sigma_{2c}}\frac{j\beta ka}{2Z_0} - \frac{jZ_0 k(1-\beta^2\epsilon_1)\sigma_{2c}(a_2-a)}{\beta\epsilon_1\kappa_{\text{TiN}}}\right]\tanh \kappa_{\text{TiN}} t + 1 + \frac{k^2(1-\beta^2\epsilon_1)a(a_2-a)}{2\epsilon_1}}{\frac{\kappa_{\text{TiN}}\tanh\kappa_{\text{TiN}} t}{\sigma_{2c}} - \frac{jZ_0 k(1-\beta^2\epsilon_1)(a_2-a)}{\beta\epsilon_1}}\right]^{-1}, \tag{B19}$$

for relativistic beams. Furthermore, if we focus on the frequency range where the skin depth δ is greater than the thickness of the titanium nitride t,

$$f < \frac{1}{\pi t^2\mu_0\sigma_{2c}}, \tag{B20}$$

typically satisfying the conditions

$$f \ll \frac{cZ_0\sigma_{2c}t}{\pi a}, \tag{B21}$$

$$f \ll \frac{c\beta}{2\pi}\sqrt{\frac{2\epsilon_1}{(\beta^2\epsilon_1 - 1)a(a_2 - a)}}, \tag{B22}$$

$$t \ll \frac{(1 - \beta^2\epsilon_1)(a_2 - a)}{\beta^2\epsilon_1}, \tag{B23}$$

the impedance of the ceramic chamber is approximated as

$$Z_{\mathrm{L,ceramic}} = \frac{Z_0 \mathcal{L}}{2\pi a \left[Z_0 \sigma_{2c} t - \frac{j\epsilon_1}{(\beta^2\epsilon_1 - 1)ka \log\left[\frac{a_2}{a}\right]} \right]}, \tag{B24}$$

which is the same as Eq. (19), when $(a_2 - a)/a$ is approximated as

$$\frac{a_2 - a}{a} \simeq \log\left[1 + \frac{a_2 - a}{a}\right], \tag{B25}$$

for $a_1 \simeq a_2$.

References

[1] B. W. Zotter and S. A. Kheifets, Impedances and Wakes in High-Energy Particle Accelerators (World Scientific Pub Co Inc, 1998),
[2] A. W. Chao, Physics of Collective Beam Instabilities in High Energy Accelerators (John Wiley and Sons, 1993),
[3] A. Burov and V. Lebedev, Proc. 8th European Particle Accelerator Conf., p. 1452 (2002).
[4] Y. Shobuda and K. Yokoya, Phys. Rev. E **66**, 056501 (2002).
[5] E. Metral, Transverse Resistive-Wall Impedance from Very Low to Very High Frequencies, CERN-AB-2005-084 (CERN, Geneva, 2005).
[6] E. Metral, B. Zotter, and B. Salvant, Proc. 22nd Particle Accelerator Conf., p. 4216 (2007).
[7] N. Mounet and E. Metral, Proc. 1st Int. Particle Accelerator Conf., p. 2039 (2010).
[8] K. Yokoya, Part. Accel. **41**, 221, (1993).
[9] R. Gluckstern and B. Zotter, Phys. Rev. Accel. Beams **4**, 024402, (2001).
[10] A. M. Al-Khateeb, R. W. Hasse, O. Boine-Frankenheim, W. M. Daqa, and I. Hofmann, Phys. Rev. Accel. Beams **10**, 064401 (2007).
[11] F. Roncarolo, F. Caspers, T. Kroyer, E. Metral, N. Mounet, B. Salvant, and B. Zotter, Phys. Rev. Accel. Beams **12**, 084401, (2009)
[12] M. Ivanyan, E. Laziev, V. Tsakanov, A. Vardanyan, S. Heifets, and A. Tsakanian, Phys. Rev. Accel. Beams **11**, 084001 (2008).
[13] M. Ivanyan, A. Grigoryan, V. Tsakanov, and M. Dehler, Proc. 23rd Particle Accelerator Conf., p. 4616 (2009).
[14] K. M. Hock and A. Wolski, Nucl. Instrum. Meth. A **657**, 94 (2011).
[15] E. Koukovini-Platia, G. Rumolo, and C. Zannini, Proc. 5th Int. Particle Accel. Conf., p. 2384 (2014).
[16] N. Mounet, N. Biancacci, and D. Amorim, ImpedanceWake2D (CERN, Geneva, 2022) (available at: https://twiki.cern.ch/twiki/bin/view/ABPComputing/ImpedanceWake2D, date last accessed April 6, 2022).
[17] Y. Shobuda, Beam no ukeru impedance to beam no fuanteisei no riron (KEK, Ibaraki, 2010) (available at: http://accwww2.kek.jp/oho/OHO%20text%20archives%202005-2011/OHO10%20web%20final/OHO10_shobuda_20100816.pdf, date last accessed April 6, 2022) [in Japanese].
[18] Y. Shobuda and T. Toyama, Phys. Rev. Accel. Beams **23**, 092801, (2020).
[19] Y. Shobuda and Y. H. Chin, Prog. Theor. Exp. Phys. **2017**, 123G01 (2017).
[20] Y. Shobuda, Prog. Theor. Exp. Phys. **2018**, 123G01 (2018).
[21] Y. Shobuda, Y. H. Chin, and K. Takata, Phys. Rev. ST Accel. Beams **12**, 094401 (2009).
[22] Y. Shobuda, Y. H. Chin, and K. Takata, Phys. Rev. Accel. Beams **17**, 091001 (2014).
[23] Y. Shobuda, Y. H. Chin, and K. Takata, Phys. Rev. ST Accel. Beams **10**, 044403 (2007).
[24] M. Abramowitz and I. Stegun, Handbook of Mathematical Functions (Dover Publications, New York, 1974).
[25] S. Lee, Simplified ZL model of the ceramic pipe in RCS, internal report (KEK, Tsukuba, 2003) (available at: http://www-accps.kek.jp/J-PARC/beam_instability/index-impedance_budget.html) [in Japanese].
[26] G. Stupakov, Phys. Rev. Accel. Beams **23**, 094401 (2020).
[27] S. Machida, AIP Conf. Proc. **297**, 459 (1993).
[28] Y. Shobuda, F. Noda, S. Machida, Y. H. Chin, K. Takata, and T. Toyama, Proc. 10th European Particle Accelerator Conf., p. 2910 (2006).

[29] Y. Shobuda and Y. H. Chin, Sci. Rep. **8**, 12805 (2018).
[30] P. K. Saha et al., Phys. Rev. Accel. Beams **21**, 024203 (2018).
[31] Y. Shobuda et al., Prog. Theor. Exp. Phys. **2017**, 013G01 (2017).
[32] L. J. Laslett, eConf **C630610**, 324 (1963).
[33] W. Panofsky and W. Wenzel, Rev. Sci. Instrum. **27**, 967 (1956).